minerals

MDPI

Article

Minor and Trace Elements in Natural Tetrahedrite-Tennantite: Effects on Element Partitioning among Base Metal Sulphides

Luke L. George [1,*], Nigel J. Cook [2] and Cristiana L. Ciobanu [2]

[1] School of Physical Sciences, The University of Adelaide, Adelaide, SA 5005, Australia
[2] School of Chemical Engineering, The University of Adelaide, Adelaide, SA 5005, Australia; nigel.cook@adelaide.edu.au (N.J.C.); cristiana.ciobanu@adelaide.edu.au (C.L.C.)
* Correspondence: luke.george@adelaide.edu.au; Tel.: +61-4-3510-1187

Academic Editor: Antonio Simonetti
Received: 21 December 2016; Accepted: 23 January 2017; Published: 29 January 2017

Abstract: Minerals of the tetrahedrite isotypic series are widespread components of base metal ores, where they co-exist with common base metal sulphides (BMS) such as sphalerite, galena, and chalcopyrite. We used electron probe microanalysis and laser-ablation inductively-coupled plasma mass spectrometry to obtain quantitative multi-trace element data on tetrahedrite-tennantite in a suite of 37 samples from different deposits with the objective of understanding which trace elements can be incorporated, at what levels of concentration, and how the presence of tetrahedrite-tennantite influences patterns of trace element partitioning in base metal ores. Apart from Fe and Zn, Hg and Pb are the two most abundant divalent cations present in the analysed tetrahedrite-tennantite (up to 10.6 wt % Hg and 4 wt % Pb). Cadmium, Co and Mn are also often present at concentrations exceeding 1000 ppm. Apart from one particularly Te-rich tetrahedrite, most contained very little Te (around 1 ppm), irrespective of prevailing assemblage. Bismuth is a common minor component of tetrahedrite-tennantite (commonly > 1000 ppm). Tetrahedrite-tennantite typically hosts between 0.1 and 1000 ppm Se, while Sn concentrations are typically between 0.01 and 100 ppm. Concentrations of Ni, Ga, Mo, In, Au, and Tl are rarely, if ever, greater than 10 ppm in tetrahedrite-tennantite and measured W concentrations are consistently <1 ppm. Taking into account the trace element concentrations in co-crystallizing BMS, the results presented allow the partitioning trends between co-crystallized sphalerite, galena, chalcopyrite, and tetrahedrite-tennantite to be defined. In co-crystallizing BMS assemblages, tetrahedrite-tennantite will always be the primary host of Ag, Fe, Cu, Zn, As, and Sb, and will be the secondary host of Cd, Hg, and Bi. In contrast, tetrahedrite-tennantite is a poor host for the critical metals Ga, In, and Sn, all of which prefer to partition to co-crystallizing BMS. This study shows that tetrahedrite-tennantite is a significant carrier of a range of trace elements at concentrations measurable using contemporary instrumentation. This should be recognized when establishing protocols for trace element analysis of tetrahedrite-tennantite, and when assessing the main hosts of trace elements in any given assemblage, e.g., for geometallurgical purposes.

Keywords: tetrahedrite-tennantite; trace elements; laser-ablation inductively-coupled plasma mass spectrometry; element partitioning

1. Introduction

The tetrahedrite isotypic series [1–4] can be expressed by the general formula $A_6(B,C)_6X_4Y_{12}Z$, where A = Cu or Ag in triangular coordination, B = Cu or Ag in tetrahedral coordination, C = Fe or Zn, or more rarely Pb, Hg, Cd or Mn also in tetrahedral coordination, X = Sb, As, or more rarely Bi or Te in

trigonal pyramidal coordination, *Y* = S or Se in tetrahedral coordination, and *Z* is S or Se in a special octahedral coordination [4], i.e., $(Cu,Ag)_6(Cu,Ag,Fe,Zn,Pb, etc.)_6(Sb,As,Bi,Te)_4(S,Se)_{13}$. Any excess of Cu above 10 atoms per formula unit (*apfu*) ("Cu-excess tetrahedrite-tennantite"; e.g., [5,6]) is taken to indicate the presence of Cu^{2+} [7]. Divalent metals are limited to 2 *apfu* in the tetrahedrite-tennantite structure [4].

The tetrahedrite isotypic series currently comprises eight named minerals: tetrahedrite ($Cu_6[Cu_4(Fe,Zn)_2]Sb_4S_{13}$), tennantite ($Cu_6[Cu_4(Fe,Zn)_2]As_4S_{13}$), freibergite ($Ag_6[Cu_4Fe_2]Sb_4S_{13-x}$), hakite ($Cu_6[Cu_4Hg_2]Sb_4Se_{13}$), giraudite ($Cu_6[Cu_4(Fe,Zn)_2]As_4Se_{13}$), goldfieldite ($Cu_{10}Te_4S_{13}$), argentotennantite ($Ag_6[Cu_4(Fe,Zn)_2]As_4S_{13}$), and argentotetrahedrite ($Ag_{10}(Fe,Zn)_2Sb_4S_{13}$; Table 1). The series is notable among sulphides for extensive fields of solid solution and broad ranges of metals that can be incorporated within the structure (e.g., [8–10]). This diversity is borne out by the range of minor and trace elements measured in natural specimens. Perhaps most noteworthy, the tetrahedrite isotypic series is an important concentrator of silver, and may also be the main host for antimony and arsenic in many ore deposits. Research interest in tetrahedrite-tennantite has also been generated by the observation of compositional variations across an orefield that may be tied to ore-forming processes (e.g., [11–14]), and which offer insights into ore genesis as well as potential as exploration vectors in, for example, porphyry-epithermal environments.

Table 1. Named minerals in the tetrahedrite isotypic series.

Mineral	Ideal Formula	References
Tetrahedrite	$Cu_6[Cu_4(Fe,Zn)_2]Sb_4S_{13}$	[1,3,15,16]
Tennantite	$Cu_6[Cu_4(Fe,Zn)_2]As_4S_{13}$	[2,7]
Freibergite	$Ag_6[Cu_4Fe_2]Sb_4S_{13-x}$	[15,17]
Hakite	$Cu_6[Cu_4Hg_2]Sb_4Se_{13}$	[18]
Giraudite	$Cu_6[Cu_4(Fe,Zn)_2]As_4Se_{13}$	[19]
Goldfieldite	$Cu_{10}Te_4S_{13}$	[20–22]
Argentotennantite	$Ag_6[Cu_4(Fe,Zn)_2]As_4S_{13}$	[23]
Argentotetrahedrite *	$Ag_{10}(Fe,Zn)_2Sb_4S_{13}$	[24]

* Argentotetrahedrite differs from freibergite in that Ag is contained within both the A and B sites as opposed to the A site only. This endmember has only been described on the basis of electron probe microanalysis (EPMA) data. A proper definition through the IMA Commission on New Minerals, Nomenclature and Classification (CNMNC) based on X-ray powder or reflectance data is required.

The tetrahedrite isotypic series is also, undeniably, one of the most thoroughly studied among the sulphides, notably in a series of articles [10,25–29] that have explored, through experiment, how minor elements are incorporated into the tetrahedrite-tennantite (fahlore) structure.

The present contribution seeks to build on these extensive foundations, using electron probe microanalysis (EPMA) and laser-ablation inductively-coupled plasma mass spectrometry (LA-ICP-MS) on a suite of 37 samples from different locations, to address two interdependent goals. Firstly, we seek to understand the range of minor and trace elements which can be incorporated into natural tetrahedrite-tennantite, including those seldom reported in the literature for either natural or synthetic specimens. Secondly, we investigate how the preferred trace element partitioning trends among the common base metal sulphides (BMS) sphalerite, galena, and chalcopyrite outlined in George et al. (2016) [30], are modified if tetrahedrite-tennantite is present in a mineral assemblage and co-crystallizes with BMS.

2. Background

2.1. Crystal Structure

Members of the tetrahedrite isotypic series are classified as sulfosalts; a group of sulphides containing As^{3+}, Sb^{3+}, Bi^{3+} or Te^{4+}, where one or more of these metalloid cations is associated with one or more metallic cations [4]. The metalloids are not bonded to the metals; both exclusively bond to

the anion S^{2-} (or more rarely Se^{2-} or Te^{2-}). They are thus distinct from sulphide minerals such as arsenopyrite (FeAsS), löllingite ($FeAs_2$), gudmundite (FeSbS) or enargite/luzonite (Cu_3AsS_4) where trivalent metalloids bond directly to Fe or Cu.

Moëlo et al. (2008) [4] classify the tetrahedrite isotypic series as sulfosalts with an excess of small (univalent) cations (Ag,Cu) relative to (As,Sb,Bi), and further sub-group them as Cu(Ag)-rich sulfosalts. The tetrahedrite isotypic series is the most complex isostructural series among sulfosalts due to the extensive iso- and heterovalent substitutions that are possible.

In Cu pure tetrahedrite (i.e., $Cu_{12}Sb_4S_{13}$), the structure is most simply understood as linked polyhedra of metal atoms about sulphur atoms [1]. The S^{2-} anion is bonded to six Cu^{2+} cations in octahedral coordination, while each S^{-} anion is coordinated tetrahedrally to two Cu^{+} cations, one Cu^{2+} cation and one Sb^{3+} cation. The angles between bonds in the tetrahedron are significantly distorted from the ideal 109.28°. Each tetrahedron shares a corner with the octahedron, while the remaining three corners of each tetrahedron share corners with two adjacent tetrahedrons (Figure 1). Antimony cations are positioned at the tetrahedron corners closest to the octahedron. The crystal structure of tennantite is analogous to that of tetrahedrite (with As substituted for Sb), although the degree of tetrahedron distortion is generally less in tennantite [2].

Additional investigations on how the tetrahedrite-tennantite structure is changed through incorporation of major elements such as Ag, Fe, Zn or Hg have been carried out (e.g., [31–34]), as has research into the possible oxidation and coordination states of such elements (e.g., [35–37]).

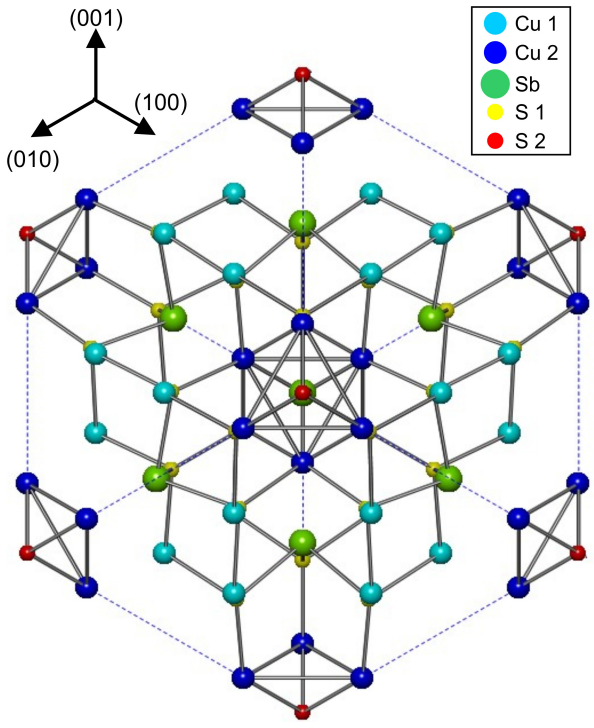

Figure 1. Crystal structure of tetrahedrite drawn from .cif file in American Mineralogist Crystal Structure Database after data in [31].

2.2. Documented Substitutions

Major metal/metalloid components of the tetrahedrite-tennantite series are copper, iron, zinc, antimony, and arsenic. Silver readily enters the tetrahedrite-tennantite structure, with argentotetrahedrite and argentotennantite the Ag end-member analogues of tetrahedrite and tennantite, respectively.

Bismuthian tetrahedrite or tennantite (the latter referred to as "*annivite*") are known from a number of localities (e.g., [38–42]), with Bi substituting into the (Sb,As) site. Staude et al. (2010) [13] document

granite-hosted tetrahedrite-tennantite containing up to 22.17 wt % (1.83 *apfu*) Bi from the Schwarzwald ore district, SW Germany. Gołębiowska et al. (2012) [43] report tetrahedrite containing up to 15.86 wt % (1.36 *apfu*) Bi and tennantite containing up to 18.41 wt % (1.51 *apfu*) Bi from Rędziny, Lower Silesia, Poland. At Rędziny, Bi-poor tennantite is generally interpreted as crystallizing at lower temperatures, with the most Bi-rich varieties crystallizing between 230 and 300 °C. Bismuth incorporation in tetrahedrite-tennantite has been studied experimentally [29], with concentrations of up to 1 *apfu* attained irrespective of the Sb/As ratio, consistent with observations in natural specimens [43].

Plumbian tetrahedrite-tennantite is also commonly reported in the literature (e.g., [44–47]). Vavelidis and Melfos (1997) [48] document 1.55 wt % Pb in tennantite, and up to 12.31 wt % Pb in tetrahedrite from the Maronia area of Thrace, Greece, and advocate that Pb^{2+} is incorporated in the (Fe,Zn) site. As much as 4.64 and 5.5 wt % Pb was measured in tennantite from Sark, Channel Islands, by Bishop et al. (1977) [49] and Ixer and Stanley (1983) [50], respectively.

Mercury is frequently reported in tetrahedrite-tennantite, where it substitutes for (Fe,Zn). Mercurian giraudite and hakite containing as much as 15.32 wt % and 14.98 wt %, respectively, are documented by Förster et al. (2002) [51] from the Niederschlema-Alberoda uranium deposit, Erzgebirge, Germany. Compositions almost span the entire solid solution range between the two minerals. They infer complete miscibility between mercurian giraudite and hakite in nature, analogous to tetrahedrite and tennantite. Jurković et al. (2011a) [52] report mercurian tetrahedrite from the Duboki Vagan barite deposit, south of Kreševo, Bosnia, containing up to 3.795 wt % Hg.

Both Mn [47,53] and Cd [54] are occasionally reported as minor elements in tetrahedrite-tennantite, substituting for (Fe,Zn). Pattrick (1978; 1985) [55,56], Huiwen and Chunpei (1988) [57] and Voudouris et al. (2011) [58] each report tetrahedrite-tennantite with Cd concentrations reaching up to ~12 wt %, representing approximately 2 *apfu* Cd. Dobbe (1992) [59] reports an unusual manganoan-cadmian tetrahedrite from Tunaberg, Bergslagen, Sweden, containing up to 2.4 wt % Mn and 5 wt % Cd.

Tellurian tetrahedrite has been widely described (e.g., [6,22] and references therein). A complete solid solution exists between tetrahedrite and the telluride-bearing end-member goldfieldite [60]. Tellurium occupies the (Sb,As) site and is incorporated through the coupled substitution $(Cu,Fe,Zn)^{2+} + (As,Sb)^{3+} = Cu^{+} + Te^{4+}$ [20,61,62]. Shimizu and Stanley (1991) [63] report tetrahedrite from the Iriki mine, Japan, with compositions varying from Te-free tetrahedrite to goldfieldite containing up to 18.5 wt % Te. Similarly, Knittel (1989) [62] measure up to 17.68 wt % Te in arsenian goldfieldite from the Marian gold mine, northern Luzon, Philippines.

Hakite and giraudite are the Se-dominant analogues of tetrahedrite and tennantite, respectively. Förster et al. (2002) [51] measure up to 39.98 wt % Se (10.86 *apfu*) and 37.55 wt % Se (11.1 *apfu*) in mercurian giraudite and hakite, respectively, from the Niederschlema-Alberoda uranium deposit, Erzgebirge, Germany. Selenium-bearing goldfieldite is reported by Pohl et al. (1996) [64] suggesting extensive solid solution among the less-common members of the tetahedrite group.

Indium-bearing tetrahedrite-tennantite is occasionally recorded (e.g., [65–68]). Gaspar (2002) [69] document up to 2.7 and 0.2 wt %. In tennantite and tetrahedrite, respectively, from Neves-Corvo, Portugal.

Tin, Co and Ni have been measured in tetrahedrite-tennantite up to a few thousand ppm. Gaspar (2002) [69] report tetrahedrite and tennantite from Neves-Corvo, Portugal, carrying up to 4784 and 1300 ppm Sn, respectively. Tetrahedrite from the same deposit contains up to 4300 ppm Co. Serranti et al. (2002) [66] also measure 4784 ppm Sn in tetrahedrite from the Corvo orebody, Portugal, as well as up to 1369 ppm Ni in tennantite. Up to 3800 ppm Co was measured in tetrahedrite-tennantite in a fluorite vein from Oberwolfach, Clara, SW Germany, and up to 6900 ppm Ni was measured from nearby Urberg, Gottesehre [13].

Gold is occasionally present in tetrahedrite-tennantite, usually only at a few ppm at most. Knittel (1989) [62], however, measured up to 0.02 wt % Au in tellurian tennantite from the Marian gold mine, northern Luzon, Philippines, while Jurković et al. (2011b) [70] record up to 39 ppm Au in mercurian tetrahedrite from the Duboki Vagan deposit, Bosnia. Wohlgemuth-Ueberwasser et al. (2015) [71] also measured up to 19.4 ppm Au in tetrahedrite-tennantite from black smokers in the Manus Basin,

Papua New Guinea, and infer that tetrahedrite-tennantite may control Au distributions in a sulphide assemblage. Unique tetrahedrite from Saski Rad, Bosnia, has also been documented containing 92 ppm Tl, 20 ppm W, 7.3 ppm Mo, and 0.5 ppm Ga, elements that are rarely if ever reported as a trace component in tetrahedrite-tennantite [70].

3. Approach and Methodology

The published data above show that alongside the essential constituents Cu, Fe, Zn, Sb, As, and S, the tetrahedrite isotypic series may incorporate up to wt % levels of Ag, Mn, Cd, Bi, Pb, In, Hg, Se, and Te, thousands of ppm Ni, Co, and Sn, at least ppm-level concentrations of Au, Tl, W, and Mo, and possibly also Ga. We have sought to analyse the concentrations of these 23 elements in a suite of 37 samples (Table 2). Sample material mostly derives from collections of the South Australian Museum and the Tate Museum (The University of Adelaide; as indicated in Table 2), while some material originates from the author's personal collections. Although some samples comprise solely tetrahedrite-tennantite (i.e., without other sulphides present), most were selected because they consist of tetrahedrite-tennantite co-existing with other base metal sulphides. Textural evidence suggests that these assemblages co-crystallized at equilibrium (~120° triple-junctions between sulphides; see Figure 2). The trace element partitioning rules for BMS outlined in George et al. (2016) [30] were employed as an additional check for assessing BMS co-crystallization. Thus through trace element analysis of the sulphides in each co-crystallized assemblage, the preferred partitioning of trace elements can be determined for a BMS assemblage comprising tetrahedrite-tennantite.

Quantitative analysis on tetrahedrite-tennantite was carried out using a Cameca SX-Five EPMA (Cameca, Gennevilliers, France), which utilizes five wavelength dispersive spectrometers (WDS). The elements analysed were S, Pb, Cd, As, Se, Fe, Cu, Mn, Ag, Sn In, Hg, Zn, Ni, Co, Sb, Te, Bi, Tl, and Ga. Beam operating conditions were maintained at 20 kV and 20 A with a beam size of 5 μm. Further details on EPMA methodology, including standards, count times and typical minimum limits of detection, are given as Electronic Appendix A. EPMA element maps were generated using the same instrument. An operating voltage of 20 kV and 224 nA were applied for EPMA mapping of selected grains, with a step size of 4 μm.

LA-ICP-MS instrumentation and analytical procedures followed those given in George et al. (2016) [30] and George et al. (in press) [72]. A Resonetics M-50-LR 193 nm Excimer laser (Resonetics, Nashua, NH, USA) and an Agilent 7700cx Quadrupole ICP mass spectrometer (Agilent, Santa Clara, CA, USA) were used for the LA-ICP-MS analysis of tetrahedrite-tennantite (Adelaide Microscopy, The University of Adelaide). An atmosphere of ultra-high purity (UHP) He (0.7 L/min) was created inside the ablation cell, and Ar (0.93 L/min) was mixed with the ablated material upon exiting the cell. The mixture then passed through a pulse-homogenizing device (squid) before being directed to the torch. Regular calibration of the ICP-MS was performed so that the sensitivity on the isotopes of interest was maximized, and formation of unwanted molecular oxide species was kept at a minimum.

Laser beam energy was kept at 100 mJ with a 26 μm spot size, while the repetition rate was maintained at 10 Hz. Each analysis was a total of 60 s, consisting of a 30 s background measurement and 30 s of sample ablation. A delay of 40 s was allowed between each analysis for cell washout and gas stabilization. The following isotopes were analysed: ^{34}S, ^{55}Mn, ^{57}Fe, ^{59}Co, ^{60}Ni, ^{65}Cu, ^{66}Zn, ^{69}Ga, ^{75}As, ^{82}Se, ^{95}Mo, ^{107}Ag, ^{111}Cd, ^{115}In, ^{118}Sn, ^{121}Sb, ^{125}Te, ^{182}W, ^{197}Au, ^{202}Hg, ^{205}Tl, ^{206}Pb, ^{207}Pb, ^{208}Pb, and ^{209}Bi. The dwell time for each element was 0.01 s, while In, Au, and Tl were set to 0.05 s. Unless tetrahedrite-tennantite was fine-grained and sparse within any given sample, we aimed to make 10 spot analyses on each sample. Electronic Appendix B shows the range of minimum detection limits and mean errors for the trace elements analysed. Electronic Appendix C shows the full tetrahedrite-tennantite LA-ICP-MS dataset, as well as the data for co-existing sphalerite, galena and chalcopyrite also analysed in each sample according to methodology outlined in George et al., (2016) [30].

Table 2. Summary of samples used in this study.

Sample	Tetrahedrite-Tennantite Composition	Assemblage	Locality	Ore Type
G16396 *	$(Cu_9,Ag_{1.2},Zn_{0.9},Fe_{0.9},Pb_{0.1})$ $(Sb_{3.8},As_{0.1})$ S_{13}	*Tet*, *Sp*, *Gn*, *Cp*	Broken Hill, NSW, Australia	SEDEX (recrystallized)
G11579 *	$(Cu_{9.6},Ag_{0.3},Zn_1,Fe_{0.9})$ $(Sb_{3.7},As_{0.2})$ $S_{13.2}$	*Tet*, *Sp*, *Cp*, *Gn*	Kalgoorlie, WA, Australia	Orogenic Au
G13289b *	$(Cu_{10.1},Zn_{1.7},Fe_{0.3})$ $(Sb_{3.2},As_{0.8})$ $S_{12.9}$	*Tet*, *Gn*, *Cp*, *Sp*	S. Wheal Exmouth, Devon, England	Low temperature replacement
G6940 *	$(Cu_{9.5},Ag_{0.5},Fe_{1.2},Zn_{0.8})$ $(Sb_{3.8},As_{0.2})$ S_{13}	*Tet*, *Cp*, *Sp*, *Gn*	Great Boulder Mine, WA, Australia	Orogenic Au
G13289a *	$(Cu_{10.1},Zn_{1.7},Fe_{0.3})$ $(Sb_{3.2},As_{0.7})$ S_{13}	*Tet*, *Cp*, *Sp*, *Gn*	S. Wheal Exmouth, Devon, England	Low temperature replacement
V446	$(Cu_{8.2},Ag_{1.9},Fe_{1.7},Zn_{0.4})$ $Sb_{3.9}$ S_{13}	*Sp*, *Gn*, *Cp*, *Tet*	Bleikvassli, Norway	SEDEX (recrystallized)
V538	$(Cu_{7.8},Ag_{2.2},Fe_{1.7},Zn_{0.4})$ $Sb_{3.9}$ $S_{13.1}$	*Sp*, *Gn*, *Cp*, *Tet*	Bleikvassli, Norway	SEDEX (recrystallized)
Hj13	$(Cu_{9.2},Ag_{0.6},Fe_{1.6},Zn_{0.4})$ $Sb_{3.9}$ $S_{13.2}$	*Gn*, *Cp*, *Sp*, *Tet*	Herja, Romania	Epithermal
G6951 *	$(Cu_{9.4},Ag_{0.5},Zn_{1.8},Cd_{0.1})$ $(Sb_{3.5},As_{0.4})$ $S_{13.2}$	*Tet*, *Sp*, *Gn*, *(Cp)*	Yerranderie, NSW, Australia	Epithermal
Bv97-52	$(Cu_9,Ag_{0.6},Fe_{1.6},Zn_{0.7},Pb_{0.2})$ $(As_{2.8},Sb_{1.5})$ $S_{13.2}$	*Ten*, *Sp*, *Gn*	Bleikvassli, Norway	SEDEX (recrystallized)
G10847 *	$(Cu_{10},Ag_{0.1},Zn_{1.7},Fe_{0.3})$ $(Sb_{2.1},As_{1.8})$ S_{13}	*Tet*, *Sp*, *Gn*	Mt. Camel, Heathcote, Vic., Australia	Greenstone hosted
EV8 **	$(Ag_{5.6},Cu_{4.6},Fe_{1.9},Zn_{0.3})$ $Sb_{3.9}$ $S_{12.6}$	*Gn*, *Sp*, *Tet*	Evelyn Mine, NT, Australia	VMS
Hj14	$(Cu_{6.8},Ag3.2,Fe_{1.8},Zn_{0.3})$ $Sb_{3.8}$ $S_{13.2}$	*Gn*, *Sp*, *Tet*	Herja, Romania	Epithermal
G6948 *	$(Cu_{9.6},Ag_{0.5},Fe_{1.4},Zn_{0.6})$ $(Sb_{3.9},As_{0.1})$ S_{13}	*Tet*, *Sp*, *Cp*, *(Gn)*	Medcritting, Tas., Australia	Unknown
G14549b *	$(Cu_{8.7},Ag1.8,Fe_{1.1},Zn_{0.7})$ $(Sb_{3.8},As_{2.8})$ $S_{12.8}$	*Tet*, *Sp*, *Cp*	Consols Mine, Broken Hill, NSW, Australia	SEDEX (recrystallized)
Mo17A	$(Cu_{7.2},Ag_{2.5},Fe_{1.6},Zn_{0.4},Pb_{0.4})$ $(Sb_{3.7},As_{0.1})$ $S_{13.1}$	*Cp*, *Gn*, *Tet*	Mofjell, Norway	SEDEX (recrystallized)
ORV1	$(Cu_{10.1},Ag_{0.1},Zn_{1.3},Fe_{0.4})$ $(Sb_{3.1},As_{0.8})$ $S_{13.2}$	*Cp*, *Gn*, *Tet*	Oravita, Romania	Skarn
G14549a *	$(Cu_{8.7},Ag_{2.4},Fe_{1.1},$ $Zn_{0.7})$ $Sb_{3.7}$ $S_{12.3}$	*Tet*, *Gn*, *(Sp)*	Consols Mine, Broken Hill, NSW, Australia	SEDEX (recrystallized)
G873 *	$(Cu_{9.5},$ $Ag_{0.7},$ $Zn_{1.2},$ $Fe_{0.7})$ $(Sb_3,As_{0.9})$ $S_{12.9}$	*Tet*, *Gn*	Yerranderrie, NSW, Australia	Epithermal
G16152 *	$(Cu_{10},Ag_{0.1},Zn_{1.1},Fe_{0.8},Co_{0.1})$ $(Sb_{2.2},As_{1.8})$ S_{13}	*Tet*, *Cp*, *(Gn)*	Siegen, Westphalia, Germany	SEDEX?
G871 *	$(Cu_{10.1},Hg_{0.9},Fe_{0.5},Zn_{0.5})$ $(Sb_{3.2},As_{0.7})$ $S_{13.1}$	*Tet*, *Cp*	Pulganbar, Grafton, NSW, Australia	Vein hosted
G874 *	$(Cu_{10.3},Zn_1,Hg_{0.5},Fe_{0.4})$ $(Sb_{3.3},As_{0.6})$ $S_{12.8}$	*Tet*, *Cp*	Pulganbar, Grafton, NSW, Australia	Vein hosted
G879 *	$(Cu_{9.6},Ag_{0.4},Fe_{1.6},Zn_{0.4})$ $(Sb_{3.8},As_{0.1})$ $S_{13.2}$	*Tet*, *Cp*	Ring Valley, Tas., Australia	Fissure fillings
G882 *	$(Cu_{10.3},Fe_1,Zn_{0.3},Hg_{0.2})$ $(Sb_{2.5},As_{1.4})$ $S_{13.1}$	*Tet*, *Cp*	Pulganbar, Grafton, NSW, Australia	Vein hosted
G6946 *	$(Cu_{10},Ag_{0.1},Zn_{1.3},Fe_{0.6})$ $(Sb_{3.7},As_{0.2})$ $S_{13.1}$	*Tet*, *Cp*	Siegen, Westphalia, Germany	SEDEX?
G6949 *	$(Cu_{9.7},Ag_{0.2},Fe_{1.7},Zn_{0.3})$ $(Sb_{3.9},As_{0.1})$ $S_{13.1}$	*Tet*, *Cp*	Webb's Ag Mine, Emmaville, NSW, Australia	Veins and dissemination
G11701 *	$(Cu_{5.2},Ag_{5.1},Fe_{1.6},Zn_{0.4})$ Sb_4 $S_{12.6}$	*Tet*, *Cp*	Broken Hill, NSW, Australia	SEDEX (recrystallized)
G14246 *	$(Cu_{9.8},Ag_{0.2},Fe_{1.5},Zn_{0.5})$ $(Sb_{3.8},As_{0.1})$ $S_{13.1}$	*Tet*, *Cp*	Curtin Davis Mine, Dundas, Tas., Australia	Intrusion related?
G14867 *	$(Cu_{10.5},Fe_{1.4},Zn_{0.2})$ $(As_{3.1},Sb_{0.8})$ S_{13}	*Ten*, *Cp*	Oraparinna, SA, Australia	Diapir related
Mo16	$(Cu_{7.3},Ag_{2.6},Fe_{1.8},Zn_{0.2})$ $(Sb_{3.8},As_{0.8})$ $S_{13.2}$	*Cp*, *Tet*, *(Gn)*	Mofjell, Norway	SEDEX (recrystallized)
G29851 *	$(Cu_{10.2},Fe_{1.1},$ $Zn_{0.5},Hg_{0.2})$ $(As_{3.6},Sb_{0.3})$ S_{13}	*Cp*, *Ten*	Gortdrum Mine, Ireland	Carbonate hosted
ORV4	$(Cu_{10.1},Zn_{1.4},Fe_{0.4})$ $(Sb_{2.7},As_{1.2})$ $S_{13.2}$	*Cp*, *Tet*	Oravita, Romania	Skarn
G12640 *	$(Cu_{10.2},Zn_{1.1},Fe_{0.9})$ $(As_{2.5},Sb_{1.4})$ $S_{12.9}$	*Ten*	Tinga, NSW, Australia	Unknown
G13301 *	$(Cu_{10.2},Fe_{1.2},Zn_{0.4})$ $(Sb_{3.3},As_{0.6})$ $S_{13.3}$	*Tet*	Allihies Mine, Castletown, Cork, Ireland	Unknown
G15977 *	$(Cu_{10.1},Zn_{1.2},Fe_{0.7})$ $(Sb_{3.2},As_{0.7})$ S_{13}	*Tet*	Mooloowatana HS, SA, Australia	Unknown
G16835 *	$(Cu_{10.1},Ag_{0.1},Zn_1,Fe_{0.7},$ $Hg_{0.1})$ $(As_2,Sb_{1.9})$ $S_{13.1}$	*Ten*	Grosskogel Mine, Austria	MVT?
VFI031 **	$(Cu_{8.4},Ag_{1.7},Zn_{1.9})$ $(Sb_{2.4},As_{1.4})$ $S_{13.1}$	*Tet*	Emperor Gold Mine, Fiji	Epithermal

Tet = tetrahedrite, *Ten* = tennantite, *Sp* = sphalerite, *Gn* = galena, *Cp* = chalcopyrite. Minerals in brackets are very minor phases. Tetrahedrite-tennantite composition determined by electron probe microanalysis. * Sample derives from the South Australian Museum. ** Sample derives from the Tate Museum. Other samples derive from the author's personal collection.

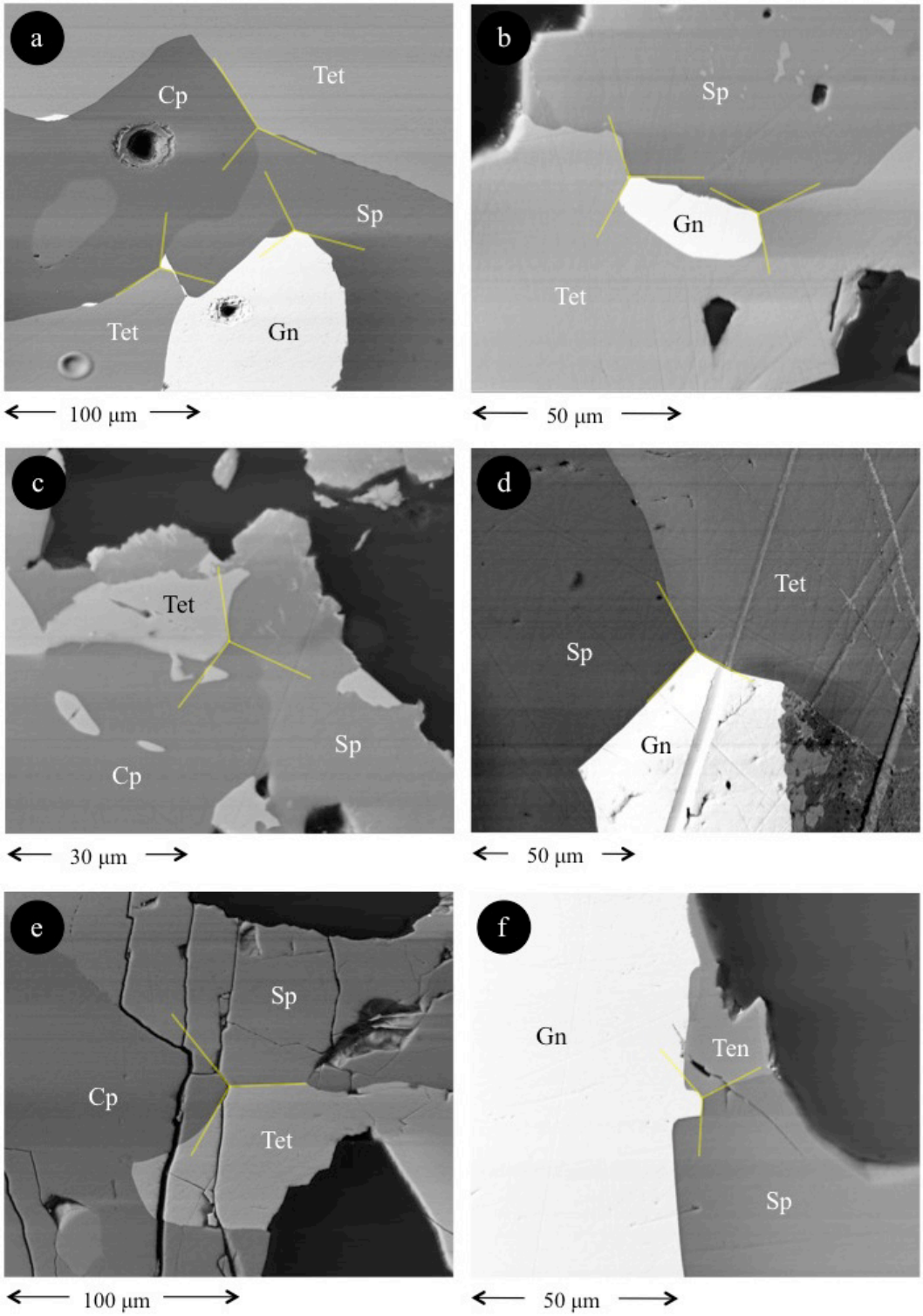

Figure 2. Representative back-scattered electron images illustrating textural evidence for tetrahedrite-tennantite and base metal sulphide (BMS) co-crystallization. (**a**) ~120° triple-junction grain boundaries as evidence for co-crystallization of tetrahedrite (Tet), sphalerite (Sp), galena (Gn) and chalcopyrite (Cp) in G11579 (Kalgoorlie, WA, Australia). Additional ~120° triple-junction grain boundaries between tetrahedrite, tennantite (Ten), sphalerite, galena, and chalcopyrite are illustrated from samples G6948 (Medcritting, Australia); (**b**,**c**) G10847 (Mt. Camel, Heathcote, Australia); (**d**) G6940 (Great Boulder Mine, WA, Australia); (**e**) and Bv97-52 (Bleikvassli, Norway); (**f**) Note grain boundaries curving towards the triple junction in order to approximate 120°.

The external standard used was MASS-1 (previously PS-1; [73]), utilizing the latest certificate of analysis [74]. Up to 10 unknown analyses were bracketed by multiple analyses of this reference material. Thus instrument drift was monitored, and a linear correction was applied to the unknown analyses. All data reduction was carried out using GLITTER [75]. Internal standardization was conducted using Cu concentration values obtained by EPMA on each individual sample. While certain interferences may have affected the reliability of some elements analysed by LA-ICP-MS (e.g., sulphur interference on ^{66}Zn; [76], or ^{59}Co^{16}O interference on ^{75}As; [77]), corrections were not applied as reliable measurements on these typically major elements were made by EPMA.

4. Results

As discussed in Cook et al. (2016) [78] and George et al. (in press) [72], mineral microanalysts are continually faced with the challenge of determining whether measurable concentrations of an element in any given mineral are present in solid solution, within microscale mineral inclusions hosted within the analysed mineral, or a mixture of both. Every effort has been made in the present study to report data that reflects elements in solid solution within the tetrahedrite-tennantite structure. This was done by examining all samples in back-scatter electron mode with a scanning electron microscope (SEM) prior to microanalysis so that only clean areas free of any noticeable inclusions were analysed. In addition, all downhole spectra from the LA-ICP-MS datasets were additionally checked for any peaks that suggest the presence of micro-inclusions beneath the sample surface (e.g., [72,79]). If present, such analyses were discarded. It is evident that some elements, notably Pb, are more commonly present as micro-inclusions in tetrahedrite-tennantite than others, perhaps due to the common presence of co-existing galena.

Table 3 summarizes the concentrations of 16 elements in tetrahedrite-tennantite as determined by EPMA. Nickel, Ga, In, and Tl were also measured, but analyses were consistently below the minimum limits of detection (average values of 0.022, 0.041, 0.031, and 0.126 wt %, respectively). Figure 3 shows the major element variation in the tetrahedrite-tennantite sample suite. Specimens spanning the entire tetrahedrite-tennantite solid solution range are represented (Figure 3a), as are samples ranging in composition from essentially Fe to Zn pure end-members (Figure 3b). Most tetrahedrite-tennantites here contain more Cu than Ag; only in sample EV8 (Evelyn Mine, NT, Australia) could freibergite be classified (Figure 3c; Table 3).

Concentrations of 20 trace and minor elements measured in tetrahedrite-tennantite by LA-ICP-MS are summarized in Table 4. Individual spot analyses are plotted as cumulative plots (Figures 4 and 5) that are sorted by the co-crystallized BMS assemblage. This allows a visualization of element concentrations and variation in different assemblages. In one sample (G871; Pulganbar, Grafton, NSW, Australia), clear oscillatory zoning was observed and mapped by EPMA (Figures 6 and 7). The zoning shows the inverse correlation between the trivalent cations Sb and As, such that Sb enriched zones are As depleted, and vice versa. Zones of high Cu, Fe, and Zn correlate with As enriched, Sb depleted zones, while high Hg zones correlate to Sb-enriched, As depleted zones. While such strong zoning appeared to be uncommon in the sample suite, other analysed tetrahedrite-tennantites may be considered as zoned to some degree based on variation of concentration values between spots. In general, grain-scale compositional zoning is common in tetrahedrite-tennantite, although this is more commonly observed as patchy heterogeneity (e.g., [80]). Micron-scale oscillatory zoning of the kind illustrated here is, however, well known from epithermal systems (e.g., [81]).

Table 3. Summary of element concentrations in tetrahedrite-tennantite determined by electron probe microanalysis (EPMA) (data in wt %).

Sample/Assemblage		S	Mn	Fe	Co	Cu	Zn	As	Se	Ag	Cd	Sn	Sb	Te	Hg	Pb	Bi	TOTAL
G16396 *	Mean (10)	24.4	0.016	3.07	-	33.3	3.59	0.237	0.021	7.25	0.051	-	27.3	-	0.069	0.994	-	100.1
Tet, Sp, Gn, Cp	*apfu*	*13.0*	*0.005*	*0.942*	-	*8.97*	*0.942*	*0.054*	*0.005*	*1.16*	*0.008*	-	*3.84*	-	*0.006*	*0.083*	-	*29.0*
G11579	Mean (10)	25.9	-	3.08	-	37.3	4.19	0.903	0.018	2.27	-	-	27.7	-	0.079	0.076	0.110	101.6
Tet, Sp, Cp, Gn	*apfu*	*13.2*	-	*0.902*	-	*9.59*	*1.05*	*0.197*	*0.004*	*0.344*	-	-	*3.72*	-	*0.006*	*0.006*	*0.009*	*29.0*
G13289b *	Mean (10)	25.5	-	1.06	-	39.5	6.71	3.47	-	0.243	-	-	23.6	-	0.076	0.066	-	100.1
Tet, Gn, Cp, Sp	*apfu*	*12.9*	-	*0.310*	-	*10.1*	*1.67*	*0.755*	-	*0.037*	-	-	*3.16*	-	*0.006*	*0.005*	-	*29.0*
G6940	Mean (10)	25.1	0.018	3.93	0.019	36.3	3.14	0.679	0.021	3.33	-	-	27.4	-	0.084	0.068	0.092	100.0
Tet, Cp, Sp, Gn	*apfu*	*13.0*	*0.005*	*1.18*	*0.005*	*9.55*	*0.801*	*0.151*	*0.004*	*0.516*	-	-	*3.76*	-	*0.007*	*0.005*	*0.007*	*29.0*
G13289a *	Mean (10)	25.7	-	0.976	-	39.4	6.77	3.20	0.031	0.212	-	-	24.1	-	0.073	0.079	-	100.4
Tet, Cp, Sp, Gn	*apfu*	*13.0*	-	*0.284*	-	*10.1*	*1.68*	*0.693*	*0.006*	*0.032*	-	-	*3.21*	-	*0.006*	*0.006*	-	*29.0*
V446	Mean (7)	24.1	0.031	5.36	0.022	30.0	1.69	-	-	11.6	-	-	27.5	0.032	0.098	0.108	-	100.5
Sp, Gn, Cp, Tet	*apfu*	*13.0*	*0.010*	*1.65*	*0.006*	*8.16*	*0.446*	-	-	*1.86*	-	-	*3.90*	*0.004*	*0.008*	*0.009*	-	*29.0*
V538	Mean (10)	24.2	0.020	5.42	0.023	28.7	1.33	-	0.033	13.5	-	0.029	27.3	-	0.100	0.086	-	100.6
Sp, Gn, Cp, Tet	*apfu*	*13.1*	*0.006*	*1.68*	*0.007*	*7.82*	*0.352*	-	*0.007*	*2.16*	-	*0.004*	*3.88*	-	*0.009*	*0.007*	-	*29.0*
Hj13	Mean (10)	25.4	0.021	5.39	0.025	35.2	1.76	-	0.025	3.88	-	0.053	28.7	-	0.118	0.088	-	100.5
Gn, Cp, Sp, Tet	*apfu*	*13.2*	*0.006*	*1.61*	*0.007*	*9.22*	*0.449*	-	*0.005*	*0.600*	-	*0.007*	*3.92*	-	*0.010*	*0.007*	-	*29.0*
G6951 *	Mean (10)	25.6	-	0.043	0.018	36.4	7.30	1.86	0.019	3.45	0.674	-	26.0	-	0.082	0.078	-	101.4
Tet, Sp, Gn, (Cp)	*apfu*	*13.2*	-	*0.013*	*0.005*	*9.44*	*1.84*	*0.408*	*0.004*	*0.526*	*0.099*	-	*3.51*	-	*0.007*	*0.006*	-	*29.0*
Bv97-52	Mean (10)	27.0	0.060	5.63	0.023	36.9	2.63	13.9	0.028	3.45	0.041	0.035	11.3	-	0.078	2.10	-	100.2
Ten, Sp, Gn	*apfu*	*13.2*	*0.017*	*1.58*	*0.006*	*9.01*	*0.650*	*2.80*	*0.006*	*0.568*	*0.005*	*0.004*	*1.53*	-	*0.006*	*0.199*	-	*29.0*
G10847	Mean (10)	26.8	-	1.00	-	40.7	6.98	8.43	-	0.745	-	-	16.6	-	0.230	0.076	-	101.6
Tet, Sp, Gn	*apfu*	*13.0*	-	*0.281*	-	*10.0*	*1.67*	*1.76*	-	*0.108*	-	-	*2.13*	-	*0.018*	*0.006*	-	*29.0*
EV8	Mean (10)	21.3	-	5.62	-	15.5	1.02	-	0.029	32.1	-	0.264	25.3	-	0.095	0.409	0.066	101.4
Gn, Sp, Tet	*apfu*	*12.6*	-	*1.91*	-	*4.63*	*0.294*	-	*0.007*	*5.64*	-	*0.042*	*3.94*	-	*0.009*	*0.038*	*0.006*	*29.0*
Hj14	Mean (6)	24.0	0.018	5.56	0.022	24.4	0.937	-	0.018	19.3	-	-	26.5	-	0.082	0.102	-	100.9
Gn, Sp, Tet	*apfu*	*13.2*	*0.006*	*1.76*	*0.007*	*6.77*	*0.253*	-	*0.004*	*3.15*	-	-	*3.85*	-	*0.007*	*0.009*	-	*29.0*
G6948	Mean (10)	24.9	0.047	4.60	-	36.3	2.33	0.234	0.027	3.39	-	-	28.1	-	0.086	0.071	0.091	100.0
Tet, Sp, Cp, (Gn)	*apfu*	*13.0*	*0.014*	*1.38*	-	*9.55*	*0.597*	*0.052*	*0.006*	*0.526*	-	-	*3.86*	-	*0.007*	*0.006*	*0.007*	*29.0*
G14549b	Mean (10)	24.0	-	3.73	-	32.5	2.66	0.134	0.017	11.1	0.147	-	27.3	-	0.094	0.255	0.129	101.7
Tet, Sp, Cp	*apfu*	*12.8*	-	*1.14*	-	*8.72*	*0.696*	*0.031*	*0.004*	*1.84*	*0.022*	-	*3.82*	-	*0.008*	*0.023*	*0.011*	*29.0*
Mo17A	Mean (7)	23.7	-	5.08	-	25.8	1.34	0.278	0.048	15.4	0.054	-	25.5	-	0.074	4.01	-	100.6
Cp, Gn, Tet	*apfu*	*13.1*	-	*1.62*	-	*7.21*	*0.363*	*0.065*	*0.012*	*2.54*	*0.009*	-	*3.73*	-	*0.007*	*0.390*	-	*29.0*
ORV1	Mean (10)	26.2	-	1.47	-	39.8	5.47	3.65	0.018	0.531	-	-	23.5	-	0.088	0.087	0.065	100.8
Cp, Gn, Tet	*apfu*	*13.2*	-	*0.427*	-	*10.1*	*1.34*	*0.783*	*0.004*	*0.079*	-	-	*3.11*	-	*0.007*	*0.007*	*0.005*	*29.0*
G14549a	Mean (10)	22.4	-	3.55	-	31.7	2.58	0.195	0.023	13.5	0.047	-	25.8	-	0.083	0.254	0.181	100.2
Tet, Gn, (Sp)	*apfu*	*12.3*	-	*1.12*	-	*8.74*	*0.694*	*0.045*	*0.005*	*2.36*	*0.008*	-	*3.73*	-	*0.007*	*0.021*	*0.016*	*29.0*
G873	Mean (10)	24.8	-	2.48	-	36.3	4.76	3.96	-	4.59	0.034	-	22.2	-	0.077	0.113	-	99.3
Tet, Gn	*apfu*	*12.9*	-	*0.740*	-	*9.52*	*1.21*	*0.881*	-	*0.710*	*0.005*	-	*3.04*	-	*0.006*	*0.009*	-	*29.0*
G16152	Mean (10)	26.6	-	2.82	0.362	40.7	4.38	8.48	-	0.449	-	-	16.8	-	0.185	0.066	-	100.9

Table 3. *Cont.*

Sample/Assemblage		S	Mn	Fe	Co	Cu	Zn	As	Se	Ag	Cd	Sn	Sb	Te	Hg	Pb	Bi	TOTAL
Tet, Cp, (Gn)	*apfu*	*13.0*	-	*0.792*	*0.096*	*10.0*	*1.05*	*1.77*	-	*0.065*	-	-	*2.17*	-	*0.014*	*0.005*	-	*29.0*
G871	Mean (10)	24.2	-	1.50	0.068	37.1	1.70	3.17	-	0.051	-	-	22.6	-	10.6	0.076	-	101.1
Tet, Cp	*apfu*	*13.1*	-	*0.464*	*0.020*	*10.1*	*0.449*	*0.726*	-	*0.008*	-	-	*3.23*	-	*0.922*	*0.006*	-	*29.0*
G874	Mean (10)	24.1	-	1.32	0.079	38.3	3.81	2.72	-	0.050	-	-	23.7	-	5.79	0.056	-	99.8
Tet, Cp	*apfu*	*12.8*	-	*0.404*	*0.023*	*10.3*	*1.00*	*0.621*	-	*0.008*	-	-	*3.33*	-	*0.494*	*0.005*	-	*29.0*
G879	Mean (10)	25.6	-	5.43	-	37.0	1.48	0.291	0.025	2.59	-	-	28.5	-	0.077	0.064	0.073	101.0
Tet, Cp	*apfu*	*13.2*	-	*1.60*	-	*9.58*	*0.371*	*0.064*	*0.005*	*0.395*	-	-	*3.85*	-	*0.006*	*0.005*	*0.006*	*29.0*
G882	Mean (10)	26.4	-	3.54	0.087	41.2	1.34	6.78	-	-	-	-	19.0	-	3.10	0.070	-	101.6
Tet, Cp	*apfu*	*13.1*	-	*1.01*	*0.024*	*10.3*	*0.327*	*1.44*	-	-	-	-	*2.50*	-	*0.247*	*0.005*	-	*29.0*
G6946	Mean (10)	25.7	-	2.05	-	39.0	5.14	1.04	0.023	0.600	-	-	27.5	-	0.158	0.059	-	101.3
Tet, Cp	*apfu*	*13.1*	-	*0.600*	-	*10.0*	*1.28*	*0.226*	*0.005*	*0.091*	-	-	*3.69*	-	*0.013*	*0.005*	-	*29.0*
G6949	Mean (10)	25.8	0.015	5.72	-	37.9	1.30	0.331	0.020	1.23	-	-	28.9	-	0.081	0.057	0.136	101.4
Tet, Cp	*apfu*	*13.1*	*0.004*	*1.67*	-	*9.75*	*0.326*	*0.072*	*0.004*	*0.186*	-	-	*3.87*	-	*0.007*	*0.005*	*0.011*	*29.0*
G11701	Mean (10)	21.5	-	4.72	0.026	17.6	1.48	-	0.025	29.2	-	-	26.1	-	0.081	0.055	-	100.6
Tet, Cp	*apfu*	*12.6*	-	*1.59*	*0.008*	*5.21*	*0.425*	-	*0.006*	*5.10*	-	-	*4.03*	-	*0.008*	*0.005*	-	*29.0*
G14246	Mean (10)	25.6	-	5.10	-	37.6	1.86	0.298	0.029	1.41	-	-	28.3	-	0.082	0.073	0.173	100.6
Tet, Cp	*apfu*	*13.1*	-	*1.50*	-	*9.76*	*0.470*	*0.065*	*0.006*	*0.215*	-	-	*3.83*	-	*0.007*	*0.006*	*0.014*	*29.0*
G14867	Mean (10)	28.0	-	5.06	0.023	44.7	0.765	15.5	0.020	0.049	-	-	6.40	-	0.392	0.073	0.135	101.0
Ten, Cp	*apfu*	*13.0*	-	*1.35*	*0.006*	*10.5*	*0.175*	*3.10*	*0.004*	*0.007*	-	-	*0.786*	-	*0.029*	*0.005*	*0.010*	*29.0*
Mo16	Mean (7)	24.3	-	5.62	0.024	26.5	0.933	3.60	0.024	15.9	0.054	-	26.7	-	0.089	0.088	-	100.6
Cp, Tet, (Gn)	*apfu*	*13.2*	-	*1.76*	*0.007*	*7.25*	*0.247*	*0.802*	*0.005*	*2.58*	*0.008*	-	*3.83*	-	*0.008*	*0.007*	-	*29.0*
G29851	Mean (10)	27.9	-	4.10	0.021	43.2	2.01	18.0	-	0.093	-	0.026	2.72	-	3.28	0.084	0.087	101.4
Cp, Ten	*apfu*	*13.0*	-	*1.10*	*0.005*	*10.2*	*0.461*	*3.60*	-	*0.013*	-	*0.003*	*0.337*	-	*0.246*	*0.006*	*0.006*	*29.0*
ORV4	Mean (10)	26.6	-	1.48	-	40.3	5.89	5.68	-	0.156	0.048	-	20.6	-	0.070	0.070	-	100.9
Cp, Tet	*apfu*	*13.2*	-	*0.419*	-	*10.1*	*1.43*	*1.20*	-	*0.023*	*0.007*	-	*2.70*	-	*0.006*	*0.005*	-	*29.0*
G12640	Mean (10)	27.1	0.017	3.46	-	42.3	4.53	12.1	-	0.212	-	-	11.2	-	0.122	0.072	-	101.1
Ten	*apfu*	*12.9*	*0.005*	*0.947*	-	*10.2*	*1.06*	*2.46*	-	*0.030*	-	-	*1.41*	-	*0.009*	*0.005*	-	*29.0*
G13301	Mean (10)	26.7	-	4.24	0.070	40.8	1.59	3.01	0.020	-	0.069	-	25.0	-	0.149	0.074	-	101.7
Tet	*apfu*	*13.3*	-	*1.21*	*0.019*	*10.2*	*0.387*	*0.639*	*0.004*	-	*0.010*	-	*3.27*	-	*0.012*	*0.006*	-	*29.0*
G15977	Mean (10)	26.0	-	2.53	-	39.8	5.07	3.45	-	0.102	0.243	-	24.2	-	0.117	0.083	-	101.3
Tet	*apfu*	*13.0*	-	*0.726*	-	*10.1*	*1.24*	*0.739*	-	*0.015*	*0.035*	-	*3.19*	-	*0.009*	*0.006*	-	*29.0*
G16835	Mean (10)	27.1	-	2.68	0.027	41.5	4.00	9.61	-	0.398	-	-	14.9	-	0.904	0.093	0.093	101.1
Ten	*apfu*	*13.1*	-	*0.746*	*0.007*	*10.1*	*0.952*	*1.99*	-	*0.057*	-	-	*1.90*	-	*0.070*	*0.007*	*0.007*	*29.0*
VFI031	Mean (5)	25.5	0.107	0.039	-	32.2	7.47	6.52	0.036	10.8	-	-	17.9	0.159	0.469	0.083	-	101.2
Tet	*apfu*	*13.1*	*0.032*	*0.011*	-	*8.37*	*1.89*	*1.43*	*0.008*	*1.65*	-	-	*2.43*	*0.020*	*0.039*	*0.007*	-	*29.0*

Tet = tetrahedrite, *Ten* = tennantite, *Sp* = sphalerite, *Gn* = galena, *Cp* = chalcopyrite, *apfu* = atoms per formula unit. Minerals in brackets are very minor phases. (X) = number of individual spot analyses in that sample. * Evidence suggests sulphides in sample did not co-crystallize (based on textures and partitioning trends among base metal sulphides). Dash = insufficient data to perform calculation (all analyses <mdl). Other <mdl values were ignored, thus data can be considered maximum concentrations. Totals are calculated by averaging the total for each spot in each sample. Hence each row will not add to the total.

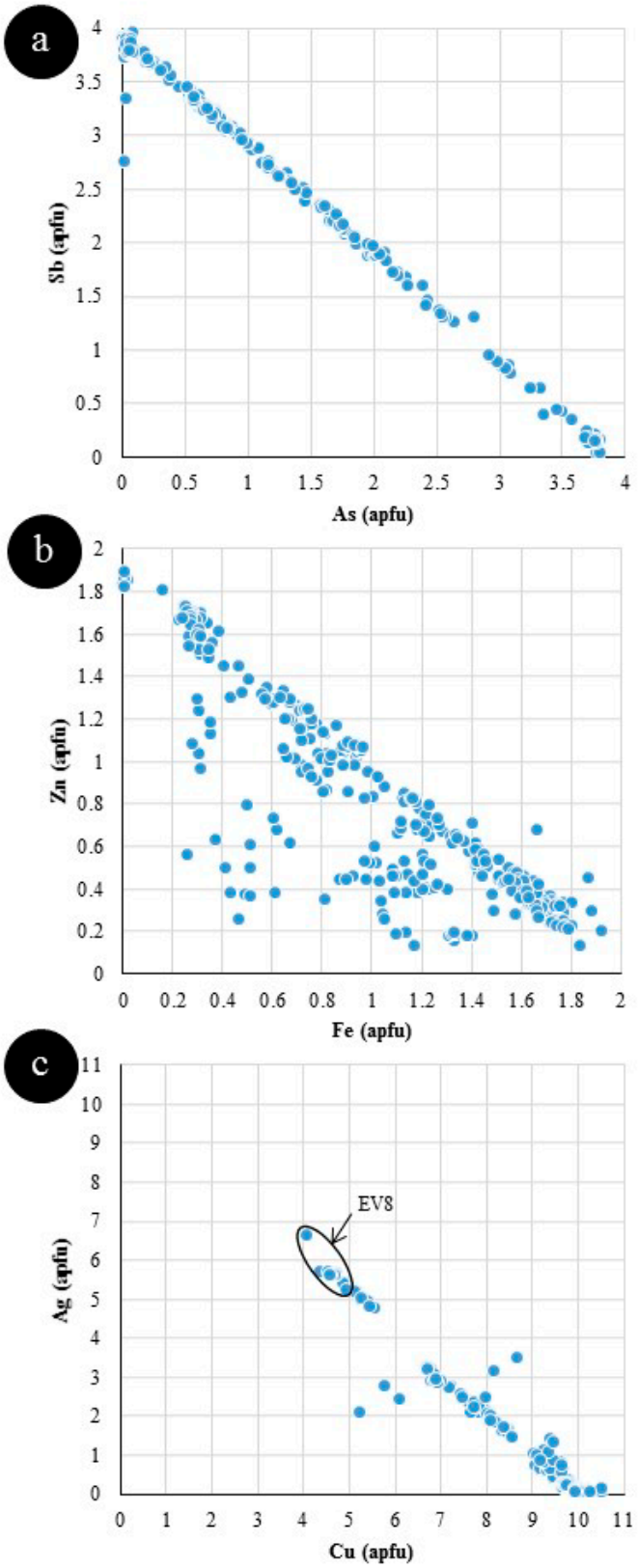

Figure 3. Scatter-plots showing the variation in major elements in the tetrahedrite-tennantite sample suite. (**a**) Sb vs. As; (**b**) Zn vs. Fe; and (**c**) Ag vs. Cu. Atoms per formula unit is calculated by normalizing mol % values to 29.

Table 4. Summary of trace element concentrations in tetrahedrite-tennantite determined by laser-ablation inductively-coupled plasma mass spectrometry (LA-ICP-MS) (data in ppm).

Sample/Assemblage		Mn	Fe	Co	Ni	Zn	Ga	As	Se	Mo	Ag	Cd	In	Sn	Te	W	Au	Hg	Tl	Pb	Bi
G16396 *	Mean (10)	1.4	ME	2.7	0.54	ME	0.09	4620	-	0.12	ME	4968	0.57	28	1.4	0.04	0.74	93	0.09	61	445
Tet, Sp, Gn, Cp	*St. Dev.*	*1.0*	*ME*	*1.1*	*0.78*	*ME*	*0.12*	*943*	*-*	*0.15*	*ME*	*751*	*0.16*	*39*	*1.1*	*0.06*	*0.53*	*20*	*0.16*	*40*	*768*
G11579	Mean (10)	32	ME	22	0.87	ME	0.06	28,446	53	0.09	ME	2692	7.0	0.54	50	-	0.03	93	0.05	3.1	3007
Tet, Sp, Cp, Gn	*St. Dev.*	*2.1*	*ME*	*4.5*	*1.0*	*ME*	*0.03*	*6725*	*23*	*0.08*	*ME*	*324*	*1.1*	*0.37*	*25*	*-*	*0.02*	*31*	*0.05*	*2.2*	*595*
G13289b *	Mean (10)	0.77	ME	44	0.14	ME	0.03	ME	11	0.03	2038	2187	0.25	0.80	0.07	0.01	0.02	9.3	0.15	270	8.2
Tet, Gn, Cp, Sp	*St. Dev.*	*0.54*	*ME*	*7.8*	*0.08*	*ME*	*0.02*	*ME*	*8.6*	*0.04*	*538*	*274*	*0.34*	*0.49*	*0.16*	*0.01*	*0.04*	*3.2*	*0.22*	*257*	*8.5*
G6940	Mean (10)	43	ME	0.55	0.33	ME	0.05	12,626	73	0.06	ME	1860	3.4	1.1	38	0.02	0.02	86	0.02	1.8	1539
Tet, Cp, Sp, Gn	*St. Dev.*	*7.9*	*ME*	*0.14*	*0.19*	*ME*	*0.04*	*5590*	*20*	*0.05*	*ME*	*231*	*0.92*	*0.71*	*21*	*0.03*	*0.02*	*28*	*0.02*	*0.68*	*142*
G13289a *	Mean (10)	0.83	10,116	38	0.25	ME	0.03	ME	21	0.04	1866	2052	0.17	0.47	0.09	0.01	0.01	13	0.05	108	11
Tet, Cp, Sp, Gn	*St. Dev.*	*0.65*	*1653*	*11*	*0.19*	*ME*	*0.03*	*ME*	*29*	*0.05*	*615*	*262*	*0.40*	*0.35*	*0.18*	*0.01*	*0.00*	*2.9*	*0.05*	*130*	*16*
V446	Mean (4)	204	ME	0.06	0.13	ME	0.19	38	12	0.02	ME	170	1.2	16	0.06	-	0.01	10	0.16	1.9	111
Sp, Gn, Cp, Tet	*St. Dev.*	*12*	*ME*	*0.05*	*0.25*	*ME*	*0.05*	*11*	*6.1*	*0.03*	*ME*	*24*	*0.21*	*1.7*	*0.09*	*-*	*0.02*	*1.5*	*0.21*	*-*	*22*
V538	Mean (3)	122	ME	0.02	0.00	ME	0.11	92	6.0	0.00	ME	158	0.64	22	0.13	-	0.00	10	0.21	21	45
Sp, Gn, Cp, Tet	*St. Dev.*	*6.9*	*ME*	*0.03*	*0.01*	*ME*	*0.10*	*44*	*2.6*	*0.00*	*ME*	*12*	*0.08*	*0.42*	*0.17*	*-*	*0.01*	*1.3*	*0.31*	*23*	*4.2*
Hj13	Mean (9)	109	ME	0.24	-	ME	0.03	117	8.9	0.08	ME	110	0.21	0.15	0.42	0.00	0.11	0.33	0.48	3.0	3.1
Gn, Cp, Sp, Tet	*St. Dev.*	*19*	*ME*	*0.38*	*-*	*ME*	*0.02*	*24*	*4.7*	*0.07*	*ME*	*18*	*0.08*	*0.23*	*0.73*	*0.01*	*0.13*	*0.10*	*0.24*	*1.4*	*1.0*
G6951 *	Mean (10)	1.5	369	27	-	ME	0.04	ME	-	0.06	ME	29,893	0.10	0.31	0.29	-	0.06	29	0.20	85	0.03
Tet, Sp, Gn, (Cp)	*St. Dev.*	*0.75*	*138*	*6.0*	*-*	*ME*	*0.02*	*ME*	*-*	*0.07*	*ME*	*7569*	*0.02*	*0.18*	*0.35*	*-*	*0.04*	*14*	*0.12*	*36*	*0.04*
Bv97-52	Mean (8)	389	ME	0.01	0.15	ME	0.32	ME	3.8	0.05	ME	682	1.9	46	-	-	0.00	46	0.00	ME	9.1
Ten, Sp, Gn	*St. Dev.*	*332*	*ME*	*0.01*	*0.37*	*ME*	*0.51*	*ME*	*1.9*	*0.05*	*ME*	*351*	*1.6*	*128*	*-*	*-*	*0.00*	*18*	*0.00*	*ME*	*5.9*
G10847	Mean (10)	18	ME	0.03	0.35	ME	0.34	ME	11	0.07	5164	1325	0.09	0.92	0.40	-	0.06	2668	0.11	13	1.3
Tet, Sp, Gn	*St. Dev.*	*4.7*	*ME*	*0.02*	*0.24*	*ME*	*0.13*	*ME*	*7.2*	*0.06*	*4579*	*169*	*0.02*	*0.78*	*0.41*	*-*	*0.09*	*493*	*0.22*	*9.3*	*0.22*
EV8	Mean (10)	7.6	ME	0.20	0.31	ME	0.21	121	19	-	ME	870	2.6	404	0.82	0.02	0.08	19	3.7	46,078	1174
Gn, Sp, Tet	*St. Dev.*	*3.0*	*ME*	*0.07*	*0.41*	*ME*	*0.11*	*142*	*16*	*-*	*ME*	*418*	*2.5*	*185*	*0.82*	*0.05*	*0.13*	*8.5*	*2.1*	*29,774*	*456*
Hj14	Mean (6)	80	ME	0.01	0.02	10,882	0.01	310	2.7	0.08	ME	161	0.05	18	0.09	-	11	0.26	0.24	39	0.03
Gn, Sp, Tet	*St. Dev.*	*22*	*ME*	*0.03*	*0.04*	*587*	*0.01*	*135*	*2.6*	*0.12*	*ME*	*22*	*0.05*	*16*	*0.15*	*-*	*5.2*	*0.09*	*0.58*	*10*	*0.06*
G6948	Mean (10)	517	ME	0.11	0.36	ME	0.06	8222	135	0.06	ME	1033	1.4	65	0.54	-	0.02	2.4	0.02	4.6	1933
Tet, Sp, Cp, (Gn)	*St. Dev.*	*71*	*ME*	*0.10*	*0.21*	*ME*	*0.06*	*5983*	*68*	*0.06*	*ME*	*89*	*0.17*	*28*	*0.47*	*-*	*0.01*	*2.6*	*0.01*	*3.9*	*621*
G14549b	Mean (10)	2.3	ME	1.2	0.56	ME	0.12	1921	11	0.10	ME	4731	0.33	19	0.14	-	0.39	47	0.83	871	475
Tet, Sp, Cp	*St. Dev.*	*1.2*	*ME*	*1.0*	*0.61*	*ME*	*0.09*	*805*	*9.0*	*0.13*	*ME*	*1272*	*0.24*	*19*	*0.18*	*-*	*0.22*	*23*	*0.58*	*775*	*386*
Mo17A	Mean (6)	0.50	ME	0.16	0.03	ME	0.01	20,439	5.8	0.03	ME	1751	0.02	0.06	0.83	-	0.06	1.9	0.12	ME	3.2
Cp, Gn, Tet	*St. Dev.*	*0.12*	*ME*	*0.20*	*0.07*	*ME*	*0.01*	*29,371*	*2.1*	*0.04*	*ME*	*373*	*0.01*	*0.06*	*0.71*	*-*	*0.10*	*1.1*	*0.15*	*ME*	*0.82*
ORV1	Mean (10)	0.18	ME	23	2.9	ME	0.04	ME	21	0.12	4023	979	0.40	0.11	0.34	-	0.01	36	0.00	4.0	12
Cp, Gn, Tet	*St. Dev.*	*0.13*	*ME*	*12*	*2.3*	*ME*	*0.05*	*ME*	*16*	*0.14*	*880*	*393*	*0.26*	*0.12*	*0.46*	*-*	*0.02*	*13*	*0.01*	*3.1*	*16*
G14549a	Mean (10)	1.4	ME	0.74	0.84	ME	0.13	3988	13	0.03	ME	3104	0.82	42	0.07	0.01	0.20	25	0.30	849	2794
Tet, Gn, (Sp)	*St. Dev.*	*0.61*	*ME*	*0.36*	*1.2*	*ME*	*0.07*	*1181*	*8.7*	*0.03*	*ME*	*929*	*1.5*	*41*	*0.10*	*0.01*	*0.13*	*11*	*0.16*	*106*	*1842*
G873	Mean (10)	1.6	ME	1.4	0.35	ME	0.09	ME	13	0.33	ME	4310	10	0.70	0.19	0.03	0.08	62	0.08	23	0.11
Tet, Gn	*St. Dev.*	*1.1*	*ME*	*2.0*	*0.25*	*ME*	*0.05*	*ME*	*11*	*0.89*	*ME*	*1422*	*1.9*	*0.37*	*0.20*	*0.03*	*0.07*	*25*	*0.09*	*5.7*	*0.10*
G16152	Mean (10)	0.47	ME	2512	12	ME	0.05	ME	13	1.9	4452	683	3.0	28	-	0.01	0.02	3456	0.02	16	29
Tet, Cp, (Gn)	*St. Dev.*	*0.32*	*ME*	*880*	*7.4*	*ME*	*0.03*	*ME*	*12*	*2.2*	*634*	*70*	*1.4*	*51*	*-*	*0.02*	*0.02*	*921*	*0.02*	*20*	*30*

Table 4. *Cont.*

Sample/Assemblage		Mn	Fe	Co	Ni	Zn	Ga	As	Se	Mo	Ag	Cd	In	Sn	Te	W	Au	Hg	Tl	Pb	Bi
G871	Mean (10)	0.46	ME	382	0.52	ME	0.04	ME	17	0.12	372	139	0.09	0.35	0.20	0.02	0.02	ME	0.02	1.8	0.25
Tet, Cp	*St. Dev.*	*0.45*	*ME*	*220*	*0.42*	*ME*	*0.03*	*ME*	*9.5*	*0.17*	*48*	*71*	*0.13*	*0.32*	*0.29*	*0.03*	*0.02*	*ME*	*0.01*	*1.4*	*0.21*
G874	Mean (10)	0.46	ME	557	0.20	ME	0.03	ME	14	0.11	206	263	1.8	0.47	0.17	0.02	0.01	ME	0.01	5.9	0.47
Tet, Cp	*St. Dev.*	*0.41*	*ME*	*397*	*0.12*	*ME*	*0.02*	*ME*	*15*	*0.07*	*40*	*157*	*1.2*	*0.35*	*0.16*	*0.02*	*0.01*	*ME*	*0.01*	*3.5*	*0.54*
G879	Mean (10)	7.1	ME	3.6	1.9	ME	0.14	8555	-	-	ME	380	15	1.4	0.29	0.04	0.09	20	0.11	18	1229
Tet, Cp	*St. Dev.*	*3.7*	*ME*	*2.6*	*2.9*	*ME*	*0.16*	*9952*	*-*	*-*	*ME*	*57*	*4.5*	*1.5*	*0.35*	*0.04*	*0.12*	*10*	*0.12*	*28*	*549*
G882	Mean (10)	0.70	ME	613	0.56	ME	0.13	ME	56	0.36	303	328	2.3	0.68	0.69	0.04	0.05	ME	0.03	37	4.8
Tet, Cp	*St. Dev.*	*0.62*	*ME*	*475*	*0.30*	*ME*	*0.10*	*ME*	*69*	*0.36*	*90*	*283*	*2.2*	*0.56*	*0.79*	*0.04*	*0.04*	*ME*	*0.04*	*40*	*3.3*
G6946	Mean (10)	1.4	ME	53	28	ME	0.14	ME	63	0.08	6202	1268	1.4	2.3	0.35	0.01	0.03	1917	0.01	7.3	98
Tet, Cp	*St. Dev.*	*1.2*	*ME*	*40*	*9.1*	*ME*	*0.09*	*ME*	*28*	*0.05*	*420*	*163*	*0.61*	*2.2*	*0.36*	*0.02*	*0.02*	*710*	*0.01*	*8.2*	*147*
G6949	Mean (10)	11	ME	0.32	2.6	ME	0.09	8922	16	0.09	ME	283	15	3.0	0.12	-	0.10	13	0.65	19	2821
Tet, Cp	*St. Dev.*	*7.9*	*ME*	*0.31*	*2.8*	*ME*	*0.07*	*2833*	*11*	*0.12*	*ME*	*47*	*5.9*	*2.5*	*0.13*	*-*	*0.08*	*4.5*	*0.39*	*15*	*1101*
G11701	Mean (10)	1.1	ME	78	0.55	ME	0.05	134	13	0.07	ME	1124	0.14	5.1	0.12	0.02	0.04	192	0.02	6.1	23
Tet, Cp	*St. Dev.*	*0.64*	*ME*	*21*	*0.56*	*ME*	*0.05*	*36*	*14*	*0.07*	*ME*	*902*	*0.05*	*7.5*	*0.22*	*0.02*	*0.06*	*91*	*0.04*	*3.0*	*23*
G14246	Mean (10)	18	ME	3.0	0.23	ME	0.06	5264	-	0.06	ME	365	7.3	1.5	0.22	0.01	0.02	58	0.08	3.2	2269
Tet, Cp	*St. Dev.*	*13*	*ME*	*1.4*	*0.13*	*ME*	*0.05*	*3493*	*-*	*0.06*	*ME*	*63*	*4.5*	*1.0*	*0.26*	*0.01*	*0.01*	*29*	*0.08*	*3.2*	*1035*
G14867	Mean (10)	0.36	ME	146	0.54	16,696	0.07	ME	376	0.15	70	183	3.0	0.68	0.34	-	0.02	5310	0.14	3.0	3768
Ten, Cp	*St. Dev.*	*0.15*	*ME*	*3.6*	*0.49*	*903*	*0.05*	*ME*	*293*	*0.12*	*20*	*19*	*0.35*	*0.44*	*0.53*	*-*	*0.01*	*3594*	*0.18*	*0.91*	*1038*
Mo16	Mean (3)	15	ME	7.0	1.7	8795	0.06	ME	11	0.01	ME	1213	0.03	0.10	2.0	-	0.02	31	0.03	2.2	2.7
Cp, Tet, (Gn)	*St. Dev.*	*6.6*	*ME*	*12*	*2.9*	*6021*	*0.09*	*ME*	*3.4*	*0.02*	*ME*	*599*	*0.01*	*0.04*	*1.2*	*-*	*0.02*	*10*	*0.06*	*1.0*	*1.0*
G29851	Mean (10)	0.88	ME	78	1.1	ME	0.10	ME	33	1.0	909	535	0.31	0.91	1.7	0.07	0.11	ME	0.12	108	1361
Cp, Ten	*St. Dev.*	*0.79*	*ME*	*28*	*0.75*	*ME*	*0.10*	*ME*	*22*	*1.0*	*382*	*97*	*0.12*	*0.77*	*1.3*	*0.07*	*0.22*	*ME*	*0.21*	*89*	*1471*
ORV4	Mean (10)	29	ME	3.3	1.9	ME	0.02	ME	12	0.19	1409	1269	4.5	0.07	3.0	-	-	37	0.01	2.9	140
Cp, Tet	*St. Dev.*	*29*	*ME*	*2.7*	*1.6*	*ME*	*0.04*	*ME*	*4.5*	*0.31*	*274*	*395*	*2.3*	*0.06*	*4.9*	*-*	*-*	*21*	*0.02*	*2.1*	*136*
G12640	Mean (10)	79	ME	3.1	0.62	ME	0.08	ME	107	0.15	1301	658	0.34	2.6	7.1	0.03	0.03	1654	0.14	7.3	54
Ten	*St. Dev.*	*13*	*ME*	*0.49*	*0.47*	*ME*	*0.06*	*ME*	*22*	*0.18*	*185*	*39*	*0.05*	*1.2*	*2.7*	*0.03*	*0.03*	*329*	*0.22*	*2.3*	*12*
G13301	Mean (10)	1.0	ME	633	31	ME	0.27	ME	127	-	158	7005	2.7	0.66	3.4	0.03	0.02	1747	0.02	11	100
Tet	*St. Dev.*	*2.2*	*ME*	*18*	*26*	*ME*	*0.20*	*ME*	*43*	*-*	*27*	*991*	*0.79*	*0.60*	*2.7*	*0.03*	*0.02*	*322*	*0.02*	*6.1*	*49*
G15977	Mean (10)	9.2	ME	19	0.28	ME	0.11	ME	32	0.06	630	1488	0.04	0.77	1.0	-	0.18	321	0.01	3.9	10.9
Tet	*St. Dev.*	*2.0*	*ME*	*2.7*	*0.16*	*ME*	*0.11*	*ME*	*15*	*0.08*	*181*	*114*	*0.03*	*0.42*	*0.73*	*-*	*0.05*	*129*	*0.02*	*2.4*	*1.0*
G16835	Mean (10)	2.0	ME	85	0.88	ME	0.11	ME	12	0.14	3942	331	1.1	0.70	1.1	0.05	0.18	14,761	0.06	61	2385
Ten	*St. Dev.*	*2.8*	*ME*	*8.4*	*0.76*	*ME*	*0.10*	*ME*	*11*	*0.13*	*314*	*45*	*0.19*	*0.65*	*1.3*	*0.12*	*0.13*	*2281*	*0.08*	*24*	*770*
VFI031	Mean (10)	1019	153	-	0.16	ME	1.2	ME	624	0.17	ME	1095	6.9	6.1	3648	0.01	2.2	8965	0.22	67	1.7
Tet	*St. Dev.*	*236*	*57*	*-*	*0.10*	*ME*	*0.42*	*ME*	*213*	*0.34*	*ME*	*129*	*2.1*	*11*	*3185*	*0.01*	*1.1*	*3439*	*0.13*	*76*	*0.11*

Tet = tetrahedrite, *Ten* = tennantite, *Sp* = sphalerite, *Gn* = galena, *Cp* = chalcopyrite, *St. Dev.* = standard deviation. Minerals in brackets are very minor phases. (X) = number of individual spot analyses in that sample. Dash = insufficient data to perform calculation (all analyses <mdl). Other <mdl values were treated as mdl/2. ME = major/minor element (concentration from EPMA > 1 wt %). * Evidence suggests sulphides in sample did not co-crystallize (based on textures and partitioning trends among base metal sulphides).

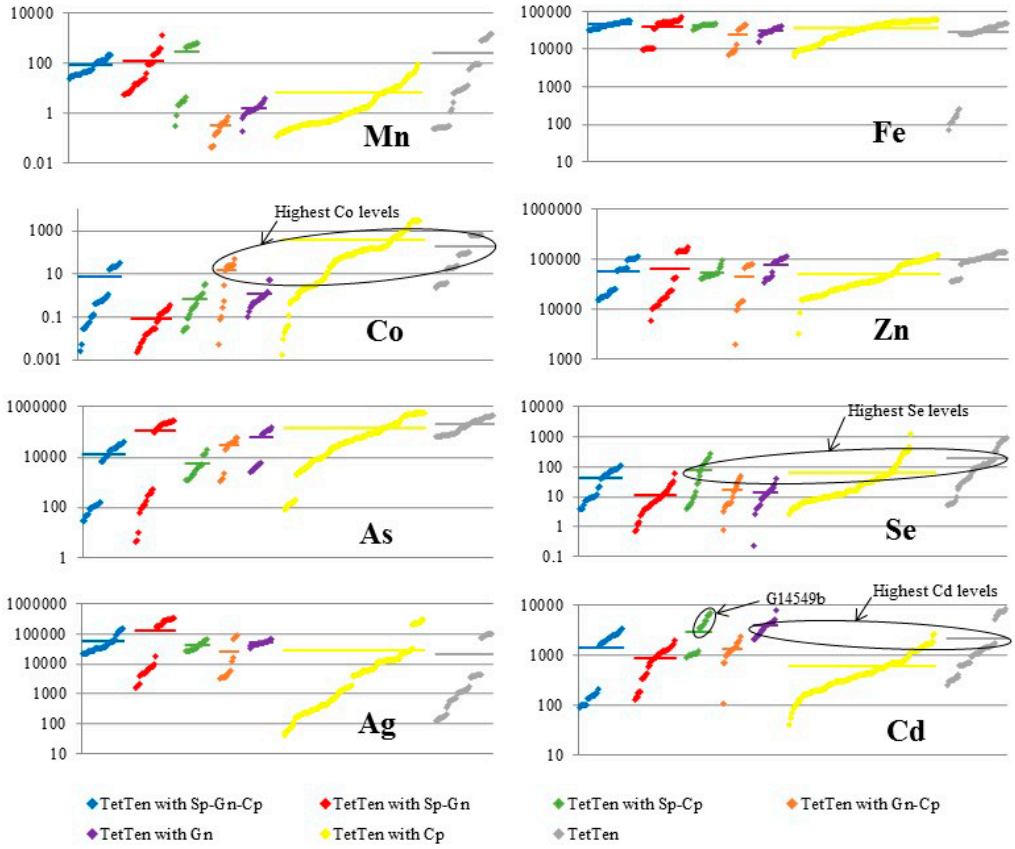

Figure 4. Cumulative plots showing individual spot concentrations of Mn, Fe, Co, Zn, As, Se, Ag and Cd in tetrahedrite-tennantite from different assemblages. Tetrahedrite-tennantite concentration data for each assemblage is sorted in ascending order and plotted in succession along the *X* axis. *Y* axis = concentration (parts per million). The average composition for each assemblage is given as a horizontal coloured line. TetTen = tetrahedrite-tennantite, Sp = sphalerite, Gn = galena, Cp = chalcopyrite.

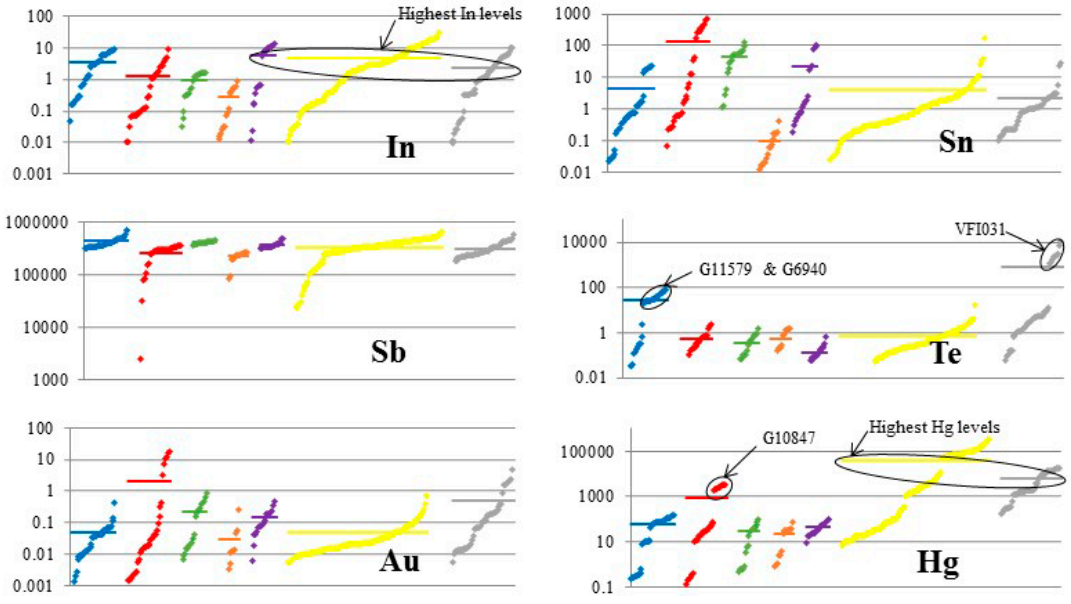

Figure 5. *Cont.*

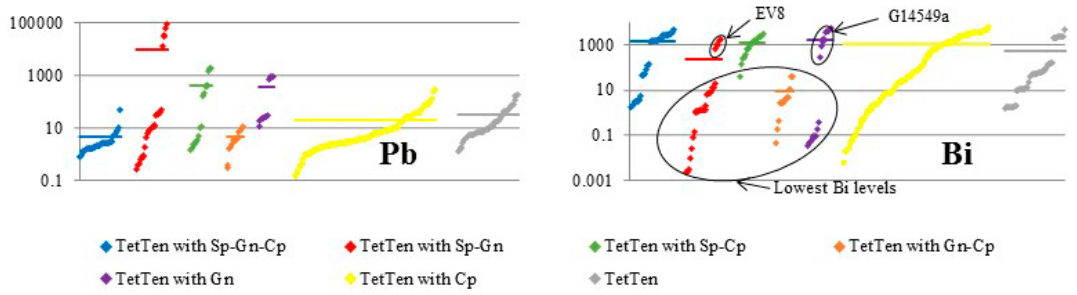

Figure 5. Cumulative plots showing individual spot concentrations of In, Sn, Sb, Te, Au, Hg, Pb, and Bi in tetrahedrite-tennantite from different assemblages. Tetrahedrite-tennantite concentration data for each assemblage is sorted in ascending order and plotted in succession along the *X* axis. *Y* axis = concentration (parts per million). The average composition for each assemblage is given as a horizontal coloured line.

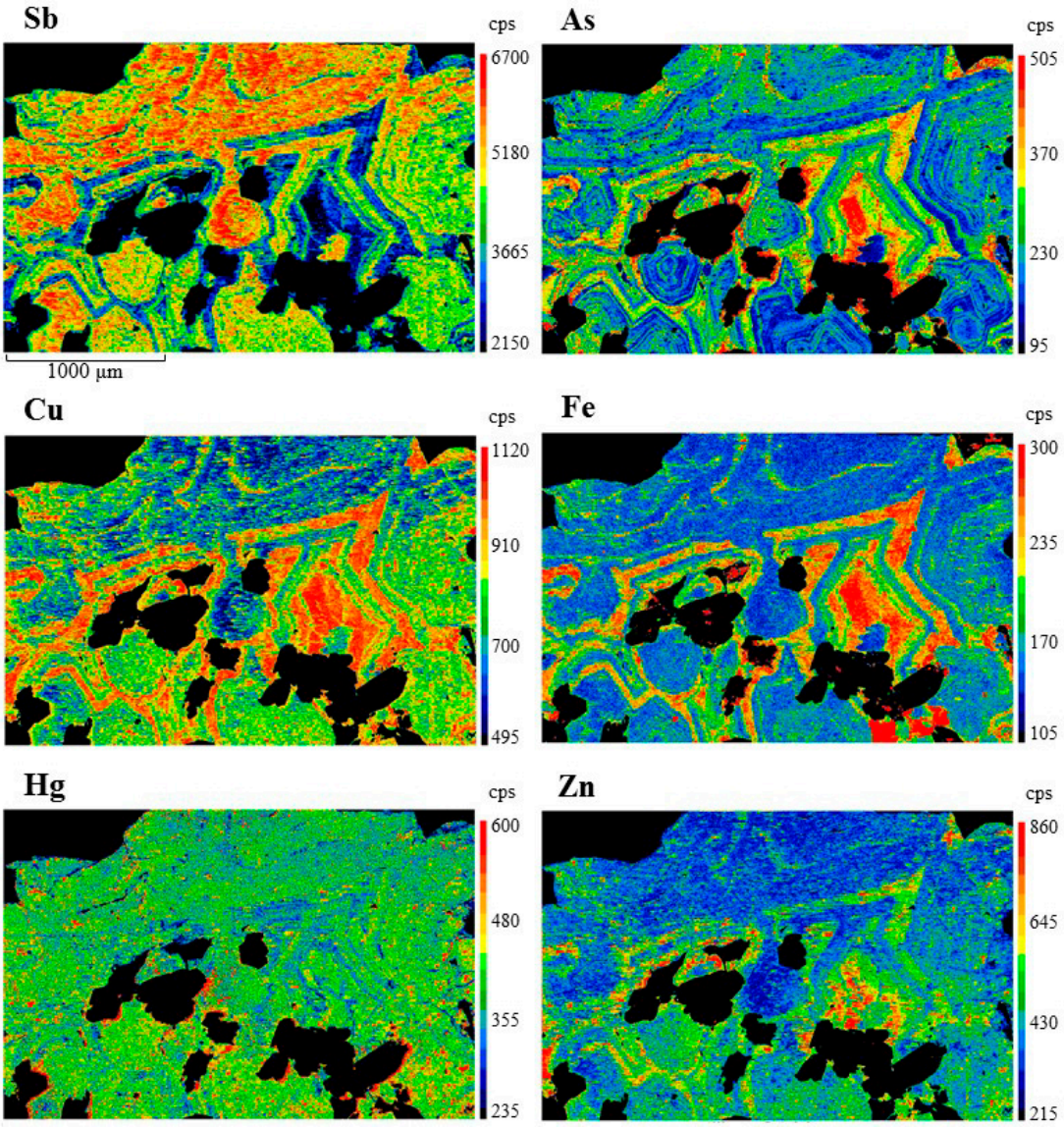

Figure 6. Electron probe microanalysis element maps showing chemical zoning of Sb, As, Cu, Fe, Hg, and Zn in tetrahedrite from sample G871 (Pulganbar, Grafton, NSW, Australia). Scales are in counts per second (cps).

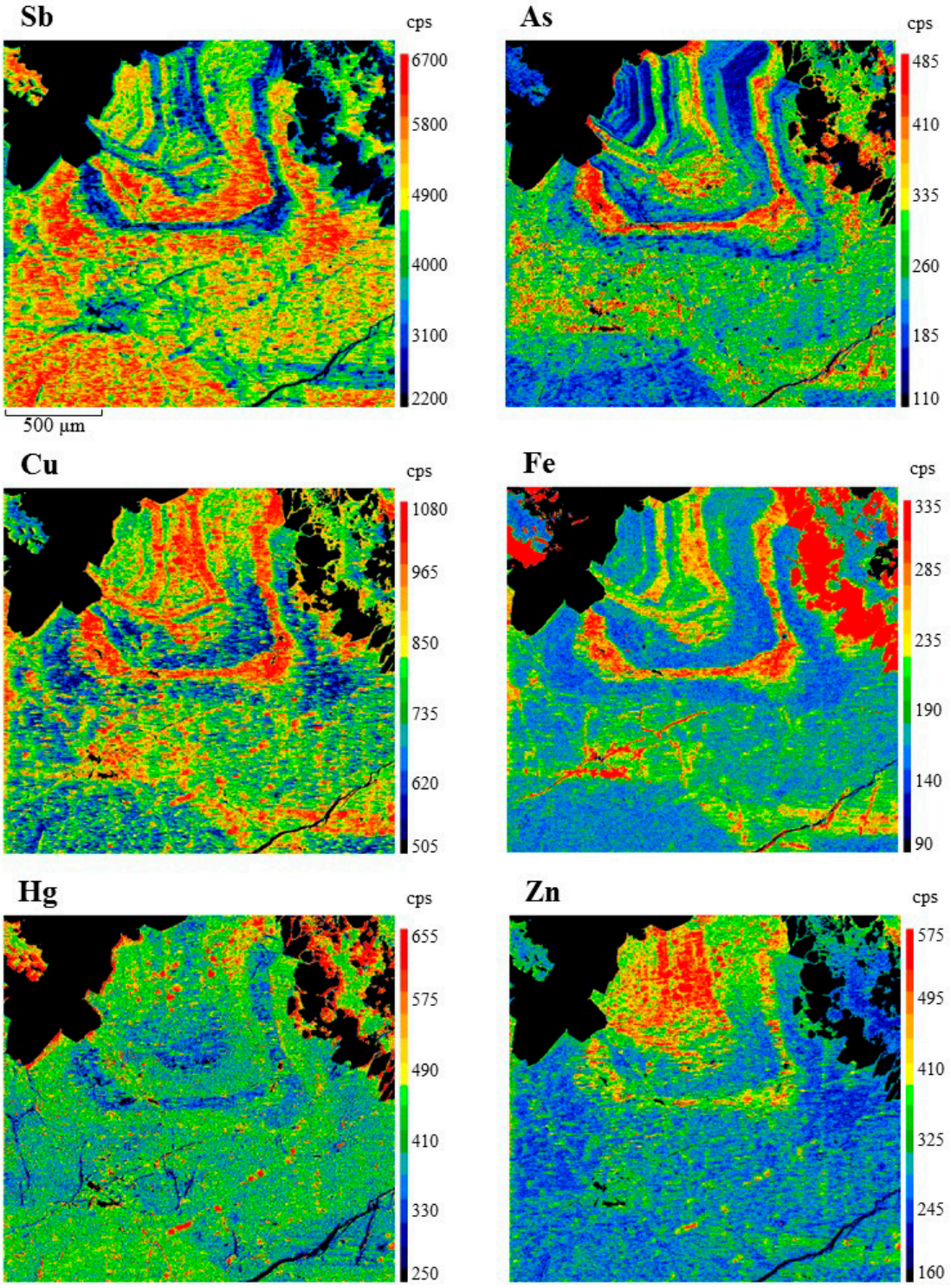

Figure 7. Electron probe microanalysis element maps showing chemical zoning of Sb, As, Cu, Fe, Hg, and Zn in tetrahedrite from sample G871 (Pulganbar, Grafton, NSW, Australia). Scales are in counts per second (cps).

Apart from Fe and Zn, Hg and Pb are the two most common divalent cations determined as present in tetrahedrite-tennantite. 10.6 wt % Hg and 4 wt % Pb are the highest measured levels of the two elements in tetrahedrite-tennantite, measured in samples G871 (Pulganbar, Grafton, NSW, Australia) and Mo17A (Mofjell, Norway), respectively. Tetrahedrite-tennantite (TetTen) crystallizing

in isolation, or with chalcopyrite (Cp; i.e., TetTen-Cp assemblages), hosts the most Hg (see Hg plot in Figure 5). While those tetrahedrite-tennantites crystallizing with sphalerite (Sp) and galena (Gn; TetTen-Sp-Gn assemblages) also host high levels of Hg, this trend is swayed by one population of Hg-rich tetrahedrites from sample G10847 (Mt. Camel, Heathcote, Australia; see Hg plot in Figure 5). The tetrahedrite in this sample co-crystallized with the most Hg-rich sphalerite of any sample here, implying a particularly Hg-rich crystallization environment. Thus, excluding this one sample, the highest Hg concentrations are present in tetrahedrite-tennantite, crystallizing without sphalerite or galena, which is in close agreement with Hg partitioning trends outlined in George et al. (2016) [30], where sphalerite is the preferred Hg host in BMS assemblages.

Cadmium, cobalt, and manganese are the other common divalent cations in tetrahedrite-tennantite. All may be present at concentrations greater than 1000 ppm. Whereas the EPMA data shows 0.674 wt % Cd in sample G6951 (Yerranderie, NSW, Australia), the LA-ICP-MS data shows almost 30,000 ppm in the same sample, hinting at heterogeneity from area to area of the sample. The highest Co and Mn in tetrahedrite-tennantite here is 0.362 wt % and 0.107 wt %, in samples G16152 (Siegen, Westphalia, Germany) and VF1031 (Emperor Gold Mine, Fiji), respectively. The LA-ICP-MS data for these samples is in close agreement. Cadmium concentrations are highest in tetrahedrite-tennantite that has not crystallized with sphalerite or chalcopyrite (see Cd plot in Figure 4). This is anticipated since Cd displays a strong preference for the sphalerite structure in BMS systems [30]. The only exception is the tetrahedrite from sample G14549b (Consols Mine, Broken Hill, NSW, Australia), which co-crystalized with sphalerite hosting up to 10,000 ppm Cd (see Cd plot in Figure 4). The exceptionally Cd-rich environment this assemblage formed in explains the high Cd concentrations in tetrahedrite, even though sphalerite co-crystallized. In a similar way, Co concentrations are also highest in those tetrahedrite-tennantites that have not crystallized with sphalerite (see Co plot in Figure 4), in line with findings reported by George et al. (2016) [30].

Tetrahedrite in sample VFI031 (Emperor Gold Mine, Fiji) contains as much as 3648 ppm Te, the highest concentration measured in this study. Apart from this sample, and two samples from the Kalgoorlie ore district, Western Australia (G11579 and G6940 with tetrahedrites containing 50 and 38 ppm Te, respectively), the mean Te concentrations in all tetrahedrite-tennantites from all assemblages are remarkably constant around the 1 ppm level (see Te plot in Figure 5).

Bismuth concentrations exceed 1000 ppm in tetrahedrite-tennantites from all assemblages except those co-crystallizing with galena and chalcopyrite, where concentrations only exceed 10 ppm in two spots. Bismuth concentrations in tetrahedrite-tennantite from TetTen-Sp-Gn and TetTen-Gn assemblages are also very low if samples EV8 (Evelyn Mine, NT, Australia) and G14549a (Consols Mine, Broken Hill, NSW, Australia) are excluded, both of which contain galena with up to 10,000 ppm Bi (see Bi plot in Figure 5). The Bi-rich galena co-crystallizing with high Bi tetrahedrite points at particularly Bi-rich crystallization environments for these samples. Such samples are anomalous for the otherwise Bi-depleted tetrahedrite-tennantites in TetTen-Sp-Gn and TetTen-Gn assemblages (see Bi plot in Figure 5). As shown in George et al. (2016) [30], the presence of galena can be considered the cause of this Bi depletion in tetrahedrite-tennantite since it is the preferred host of Bi in BMS assemblages.

Tetrahedrite-tennantite typically hosts between 0.1 and 1000 ppm Se. The most Se-rich tetrahedrite is recorded in sample VFI031 (Emperor Gold Mine, Fiji; 624 ppm). In general, the highest levels of Se in tetrahedrite-tennantite are reached when galena does not co-crystallize; i.e., from TetTen, TetTen-Sp-Cp, and TetTen-Cp assemblages (see Se plot in Figure 4). This is to be expected since galena is always the preferred host of Se in BMS assemblages [30].

Tin concentrations in tetrahedrite-tennantite are usually an order of magnitude lower than those of Se (typically between 0.01 and 100 ppm); they are the highest in EV8 (Evelyn Mine, NT, Australia; 404 ppm). Interestingly, the EPMA data records up to 0.264 wt % Sn in the tetrahedrite from EV8, though this may be due to inclusions of a Sn-rich phase (possibly stannite), since some were recognized on LA-ICP-MS downhole spectra from this sample.

The concentrations of Ni, In, Au, Tl, Mo and Ga are rarely, if ever, greater than 10 ppm in tetrahedrite-tennantite. The highest mean concentrations for these elements in tetrahedrite-tennantite are 31 ppm Ni (G13301; Allihies Mine, Castletown, Cork, Ireland), 15 ppm In (G879; Ring Valley, Tas., Australia, and G6949; Webb's Ag Mine, Emmaville, NSW, Australia), 11 ppm Au (Hj14; Herja, Romania), 3.7 ppm Tl (EV8; Evelyn Mine, NT, Australia), 1.9 ppm Mo (G16152; Siegen, Westphalia, Germany) and 1.2 ppm Ga (VFI031; Emperor Gold Mine, Fiji). Measured W concentrations never exceeded 1 ppm. The highest In concentrations are recorded in tetrahedrite-tennantites that crystallize without any sphalerite observed nearby (excluding 4-component assemblages); i.e., in TetTen-Gn, TetTen-Cp and TetTen assemblages (see In plot in Figure 5). This is concordant with George et al. (2016) [30] where sphalerite was shown to be the typical preferred host of In.

5. Discussion

5.1. Element Partitioning Between Tetrahedrite-Tennantite, Sphalerite, Galena, and Chalcopyrite

Figure 8 is a series of tri-plots that show where various elements are hosted in co-crystallized three-component assemblages in which one component is tetrahedrite-tennantite. Each individual point is a sample average, and where it plots shows how much of a given element is contained within the sulphides of that assemblage as a fraction of the overall amount of that element in the assemblage (using molar percentages for comparisons between sulphides). For example, in TetTen-Sp-Gn assemblages, sphalerite always concentrates more than 60% of the Mn budget, no more than 40% is ever contained in tetrahedrite-tennantite, and co-crystallizing galena essentially contains none of the available Mn. In the TetTen-Sp-Cp assemblage, sphalerite again always concentrates >50% of the Mn budget. We can thus say that whenever sphalerite is present, it is always the primary Mn host.

Apart from cases where chalcopyrite (or other Fe-sulphides such as pyrite and pyrrhotite) co-crystallizes, Fe is always hosted in either tetrahedrite-tennantite or sphalerite. In most cases tetrahedrite-tennantite is the primary host, but in four TetTen-Sp-Gn assemblages, sphalerite hosts > 50% of the Fe budget. Cobalt does not have a strong affiliation with any of the four sulphides, although it is never primarily hosted in chalcopyrite. In the absence of sphalerite, Zn always partitions to tetrahedrite-tennantite. Gallium seems to be most affiliated with sphalerite, although in TetTen-Sp-Cp assemblages, chalcopyrite hosts the larger share of Ga in four samples. Two of these samples (V446 and V538) come from the Bleikvassli deposit, Norway, a sedimentary-exhalative deposit which is interpreted to have recrystallized at conditions of granulite facies [82,83]. The other two (G6940 and G11579) come from Kalgoorlie, Western Australia, where Boulter et al. (1987) [84] describe recrystallization of pyrite during deformation associated with regional metamorphism. Thus, those assemblages in which chalcopyrite hosts more Ga than sphalerite, both come from environments where sulphides have recrystallized under regional metamorphism. Such conditions result in chalcopyrite becoming the primary Ga host, distinct from lower temperature/pressure environments where sphalerite is the preferred host [30,72].

Selenium is always concentrated in galena whenever that mineral is present, and tetrahedrite-tennantite seems to be the secondary host in most cases. Tetrahedrite-tennantite typically hosts > 90% of the Ag budget whenever it co-crystallizes with any combination of BMS. In all but one sample, Cd is principally hosted in sphalerite when present. In the single exception (sample G10847; Mt. Camel, Heathcote, Australia), tetrahedrite-tennantite is the preferred host. The same is true in assemblages in which sphalerite is absent.

As is the case in the three-component Sp-Gn-Cp assemblage, Sn does not have a strong affiliation with any sulphide [30]. It is concentrated in different phases in different samples. In most cases, however, Sn seems to prefer the BMS over tetrahedrite-tennantite. Tellurium has a strong affiliation with galena, while Hg appears to be preferentially incorporated into either sphalerite or tetrahedrite-tennantite in different samples. Galena will concentrate Bi whenever it is present, and in its absence tetrahedrite-tennantite always becomes the primary host.

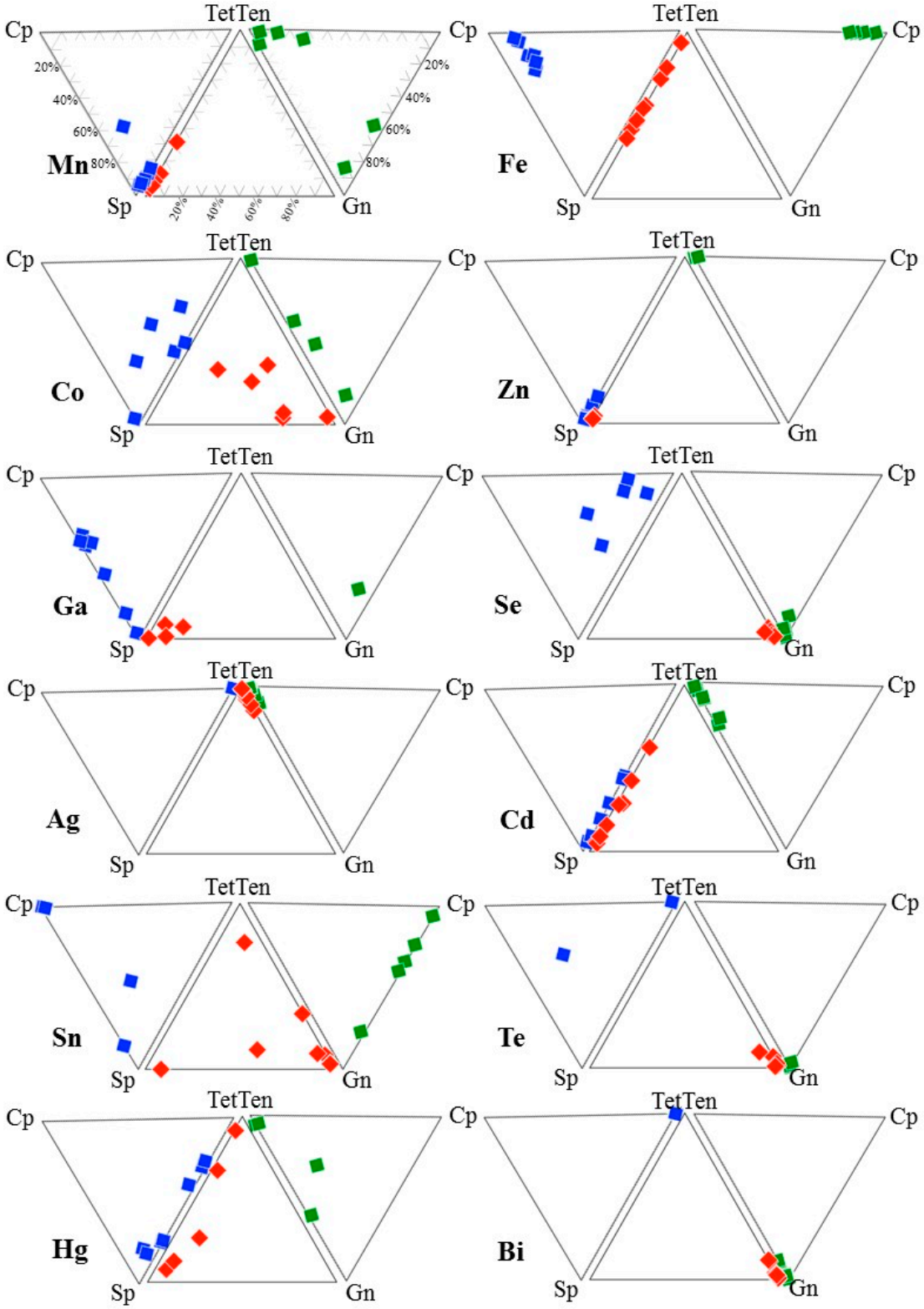

Figure 8. Series of tri-plots that show where the Mn, Fe, Co, Zn, Ga, Se, Ag, Cd, Sn, Te, Hg, and Bi budget is hosted in co-crystallized three-component assemblages comprising tetrahedrite-tennantite. Each individual point is a sample, and where it plots shows how much of a given element is contained within the sulphides of that assemblage as a fraction of the overall amount of that element in the assemblage (using molar percentages for comparisons between sulphides). TetTen = tetrahedrite-tennantite, Sp = sphalerite, Gn = galena, Cp = chalcopyrite.

5.2. Controls on Fe and Hg Partitioning

Both tetrahedrite-tennantite and sphalerite may be the primary host phase for Fe and Hg in different samples (excluding, of course, samples containing Fe-sulphides). Which mineral will host a greater molar percentage of Fe or Hg in a given system seems to depend on the amount of that element available in the system. In systems with lesser Fe, tetahedrite-tennantite is the primary Fe host, indicating that Fe prefers to partition into tetrahedrite-tennantite relative to sphalerite (Figure 9a). Sphalerite is the primary host of Fe only in those systems where Fe concentrations in tetrahedrite-tennantite approach 2 *apfu*, i.e., the maximum concentration of Fe allowed in the tetrahedrite-tennantite structure ([4]; Figure 9b). Thus, in assemblages free of Fe-sulphides, if there is more Fe than can be incorporated by tetrahedrite-tennantite, then the excess will partition to sphalerite such that sphalerite may host more Fe than tetrahedrite-tennantite.

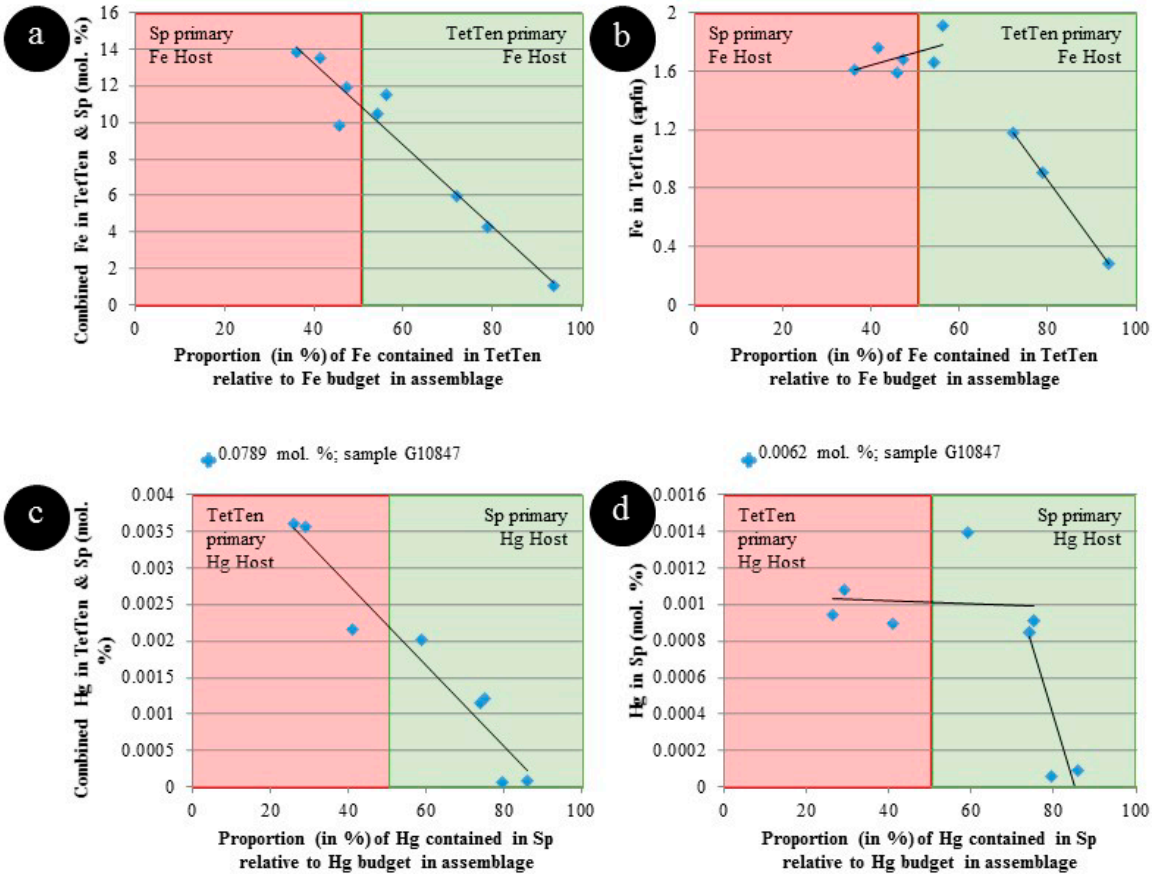

Figure 9. Scatter-plots that show the primary host of Fe and Hg depends on the concentration of Fe and Hg in tetrahedrite-tennantite and sphalerite. (**a**) Fe in tetrahedrite-tennantite and sphalerite vs. Fe in tetrahedrite-tennantite as a % of the assemblage Fe budget. (**b**) Fe in tetrahedrite-tennantite vs. Fe in tetrahedrite-tennantite as a % of the assemblage Fe budget. (**c**) Hg in tetrahedrite-tennantite and sphalerite vs. Hg in sphalerite as a % of the assemblage Hg budget. (**d**) Hg in sphalerite vs. Hg in sphalerite as a % of the assemblage Hg budget. TetTen = tetrahedrite-tennantite, Sp = sphalerite.

Similar patterns are observed for Hg. In systems with lesser Hg, sphalerite is the primary Hg host, indicating that Hg preferentially partitions into sphalerite (Figure 9c). Tetrahedrite-tennantite is the primary host of Hg only in those systems where Hg concentrations in sphalerite are ~0.001 mol% (Figure 9d). The present dataset may thus indicate that this is an approximate upper limit to Hg concentrations in sphalerite, at least when co-crystallizing with tetrahedrite-tennantite. Only in one sample is the concentration of Hg in sphalerite significantly higher than this; sample G10847

(Mt. Camel, Heathcote, VIC, Australia) which concentrates 0.0062 mol% Hg in sphalerite (equivalent to ~250 ppm Hg), and where co-crystallizing tetrahedrite hosts more than 0.07 mol% Hg (>2500 ppm Hg equivalent). This is the most Hg in any tetrahedrite-tennantite co-crystallizing with sphalerite analysed here. This particularly Hg-rich system seems to allow for exceptional Hg concentrations in sphalerite. In any case, if a given system contains more Hg than can be incorporated by sphalerite, then the excess will partition to tetrahedrite such that tetrahedrite may host more Hg than sphalerite.

6. Implications and Conclusions

This study shows that tetrahedrite-tennantite is a significant carrier of a range of trace elements at concentrations measurable using contemporary instrumentation. This should be recognized when establishing protocols for trace element analysis of tetrahedrite-tennantite, and when assessing the primary hosts for trace elements of interest in any given assemblage, e.g., for geometallurgical purposes. Most noteworthy, tetrahedrite-tennantite will always be the primary host of Ag in co-crystallizing BMS assemblages. Iron, Cu, Zn, As, Cd, Sb, Hg, and Bi are the additional elements that are controlled to some degree by the presence of tetrahedrite-tennantite. In contrast, tetrahedrite-tennantite does not appear, from the data here, to be a very good host for the critical metals Ga, In, and Sn, all of which prefer to partition to co-crystallizing BMS.

As an extension of arguments put forward by George et al. (2016) [30], the partitioning trends outlined here may be used as a tool to assess co-crystallization of a given TetTen ± Sp ± Gn ± Cp assemblage. If the hosts of various trace elements in such an assemblage do not match the preferred hosts outlined in Table 5, then it strongly suggests that assemblage did not co-crystallize. On the other hand, if the primary hosts do match those given here, that is typically suggestive of a co-crystallized assemblage.

Table 5. Preferred hosts of various trace elements in a co-crystallizing TetTen-Sp-Gn-Cp assemblage.

Trace Element	**Mn**	**Fe**	**Cu**	**Zn**
Preferred Host	Sp [1]	TetTen >Sp [3]	TetTen >Sp [3]	TetTen [1]
Trace Element	**Ga**	**As**	**Se**	**Ag**
Preferred Host	Sp [2]	TetTen >Gn [1]	Gn [1]	TetTen >Gn [1]
Trace Element	**Cd**	**In**	**Sn**	**Sb**
Preferred Host	Sp >TetTen [3]	Sp > Cp [2]	? *	TetTen >Gn [1]
Trace Element	**Te**	**Hg**	**Tl**	**Bi**
Preferred Host	Gn [1]	Sp >TetTen [3]	Gn [1]	Gn >TetTen [1]

Abbreviations: TetTen = tetrahedrite-tennantite, Sp = sphalerite, Gn = galena, Cp = chalcopyrite. [1] Trend observed in all examined samples. [2] Recrystallization increases element concentration in Cp and may make Cp primary host. [3] Trend generally, yet not always, true. * Recrystallization increases Sn concentration in Cp such that Cp is usually primary host in recrystallized samples. Below recrystallization conditions, no trend is observed.

Supplementary Materials: The following are available online at www.mdpi.com/2075-163X/7/2/17/s1.

Acknowledgments: We are deeply grateful to Ben Grguric and Ben McHenry for providing relevant sample material from the South Australian Museum. Similarly, Anthony Milnes is thanked for providing access to Tate Museum collections. We are also appreciative of microanalysis support from Ben Wade and Aoife McFadden.

Author Contributions: Nigel J. Cook conceived the research within the framework of Luke L. George's Ph.D. project. Luke L. George acquired the samples, performed all analytical work reported here, and interpreted the data. Luke L. George, and Nigel J. Cook wrote the paper with contributions from Cristiana L. Ciobanu.

Conflicts of Interest: The authors declare no conflict of interest.

References

1. Wuensch, B.J. The crystal structure of tetrahedrite, $Cu_{12}Sb_4S_{13}$. *Zeitschrift Krist. Cryst. Mater.* **1964**, *119*, 437–453. [CrossRef]
2. Wuensch, B.J.; Tackeuchi, Y.; Nowacki, W. Refinement of the crystal structure of binnite, $Cu_{12}As_4S_{13}$. *Zeitschrift Krist. Cryst. Mater.* **1966**, *123*, 1–20. [CrossRef]

3. Makovicky, E.; Skinner, B. Studies of the sulfosalts of copper. VII. Crystal structures of the exsolution products $Cu_{12.3}Sb_4S_{13}$ and $Cu_{13.8}Sb_4S_{13}$ of unsubstituted synthetic tetrahedrite. *Can. Mineral.* **1979**, *17*, 619–634.
4. Moëlo, Y.; Makovicky, E.; Mozgova, N.N.; Jambor, J.L.; Cook, N.J.; Pring, A.; Paar, W.; Nickel, E.H.; Graeser, G.; Karup-Møller, S.; et al. Sulfosalt systematics: A review. Report of the sulfosalt sub-committee of the IMA commission on ore mineralogy. *Eur. J. Mineral.* **2008**, *20*, 7–46. [CrossRef]
5. Repstock, A.; Voudouris, P.; Kolitsch, U. New occurrences of watanabeite, colusite, "arsenosulvanite" and "Cu-excess" tetrahedrite-tennantite at the Pefka high-sulfidation epithermal deposit, northeastern Greece. *Neues Jahrb. Miner. Abh. J. Miner. Geochem.* **2015**, *192*, 135–149. [CrossRef]
6. Repstock, A.; Voudouris, P.; Zeug, M.; Melfos, V.; Zhai, M.; Li, H.; Kartal, T.; Matuszczak, J. Chemical composition and varieties of fahlore-group minerals from Oligocene mineralization in the Rhodope area, Southern Bulgaria and Northern Greece. *Mineral. Petrol.* **2016**, *110*, 103–123. [CrossRef]
7. Makovicky, E.; Karanović, L.; Poleti, D.; Balić-Žunić, T.; Paar, W.H. Crystal structure of copper-rich unsubstituted tennantite, $Cu_{12.5}As_4S_{13}$. *Can. Mineral.* **2005**, *43*, 679–688. [CrossRef]
8. Sack, R.O.; Loucks, R.R. Thermodynamic properties of tetrahedrite-tennantites: Constraints on the interdependence of the Ag ↔ Cu, Fe ↔ Zn, Cu ↔ Fe, and As ↔ Sb exchange reactions. *Am. Mineral.* **1985**, *70*, 1270–1289.
9. Johnson, N.E.; Craig, J.R.; Rimstidt, J.D. Compositional trends in tetrahedrite. *Can. Mineral.* **1986**, *24*, 385–397.
10. Makovicky, E.; Karup-Möller, S. Exploratory studies on substitution of minor elements in synthetic tetrahedrite. Part I. Substitution by Fe, Zn, Co, Ni, Mn, Cr, V and Pb. Unit-cell parameter changes on substitution and the structural role of "Cu^{2+}". *Neues Jahrb. Miner. Abh.* **1994**, *167*, 89–123.
11. Hackbarth, C.J.; Petersen, U. A fractional crystallization model for the deposition of argentian tetrahedrite. *Econ. Geol.* **1984**, *79*, 448–460. [CrossRef]
12. Kovalenker, V.A.; Bortnikov, N.S. Chemical composition and mineral associations of sulphosalts in the precious metal deposits from different geological environment. *Geol. Carpathica* **1985**, *36*, 283–291.
13. Staude, S.; Mordhorst, T.; Neumann, R.; Prebeck, W.; Markl, G. Compositional variation of the tennantite-tetrahedrite solid-solution series in the Schwarzwald ore district (SW Germany): The role of mineralization processes and fluid source. *Mineral. Mag.* **2010**, *74*, 309–339. [CrossRef]
14. Apopei, A.I.; Damian, G.; Buzgar, N.; Buzatu, A. Mineralogy and geochemistry of Pb-Sb/As-sulfosalts from Coranda-Hondol ore deposit (Romania)—Conditions of telluride deposition. *Ore Geol. Rev.* **2016**, *72*, 857–873. [CrossRef]
15. Peterson, R.C.; Miller, I. Crystal structure and cation distribution in freibergite and tetrahedrite. *Mineral. Mag.* **1986**, *50*, 717–721. [CrossRef]
16. Pfitzner, A.; Evain, M.; Petricek, V. $Cu_{12}Sb_4S_{13}$: A temperature-dependent structure investigation. *Acta Cryst.* **1997**, *B53*, 337–345. [CrossRef]
17. Rozhdestvenskaya, I.V.; Zayakina, N.V.; Samusikov, V.P. Crystal structure features of minerals from the tetrahedrite-freibergite series. *Mineral. Zhurnal* **1993**, *15*, 9–17. (In Russian)
18. Johan, Z.; Kvaček, M. La hakite, un nouveau minéral du groupe de la tétraédrite. *Bull. Soc. Fr. Minéral.* **1971**, *94*, 45–48. (In French)
19. Johan, Z.; Picot, P.; Ruhlmann, F. Evolution paragénétique de la minéralisation uranifère de Chaméane (Puy-de-Dôme) France: Chaméanite, geffroyite et giraudite, trois séléniures nouveaux de Cu, Fe, Ag, and As. *Tscher. Miner. Petrog. Mitt.* **1982**, *29*, 151–167. (In French) [CrossRef]
20. Kalbskopf, R. Synthese und Kristallstruktur von $Cu_{12-x}Te_4S_{13}$, dem Tellur-Endglied der Fahlerze. *Tscher. Miner. Petrog. Mitt.* **1974**, *21*, 1–10. (In German) [CrossRef]
21. Dmitrieva, M.T.; Bojik, G.B. The crystallochemical mechanism of formation of vacancies in goldfieldite structure. *Zeitschrift Krist.* **1988**, *185*, 601.
22. Trudu, A.G.; Knittel, U. Crystallography, mineral chemistry and chemical nomenclature of goldfeldite, the tellurian member of the tetrahedrite solid-solution series. *Can. Mineral.* **1998**, *36*, 1115–1137.
23. Spiridonov, E.M.; Sokolova, N.F.; Gapeyev, A.K.; Dashevskaya, D.M.; Yevstigneyeva, T.L.; Chvileva, T.N.; Demidov, V.G.; Balashov, Y.P.; Shul'ga, V.I. The new mineral argentotennantite. *Dokl. Akad. Nauk SSSR* **1986**, *290*, 206–210. (In Russian)
24. Zhdanov, Y.Y.; Amuzinskii, V.A.; Andrianov, N.G. Discovery of a natural Ag-rich fahlore with the highest parameter of the unit cell. *Dokl. Akad. Nauk SSSR* **1992**, *326*, 337–340. (In Russian)

25. Karup-Møller, S. Exploratory studies on element substitutions in synthetic tetrahedrite. Part V. Mercurian tetrahedrite. *Neues Jahrb. Miner. Abh.* **2003**, *179*, 73–83. [CrossRef]
26. Karup-Møller, S.; Makovicky, E. Exploratory studies of element substitutions in synthetic tetrahedrite. Part II. Selenium and tellurium as anions in Zn-Fe tetrahedrites. *Neues Jahrb. Miner. Abh.* **1999**, *9*, 385–399.
27. Karup-Møller, S.; Makovicky, E. Exploratory studies of the solubility of minor elements in tetrahedrite: VI. Zinc and the combined zinc-mercury and iron-mercury substitutions. *Neues Jahrb. Miner. Mon.* **2004**, *11*, 508–524. [CrossRef]
28. Hansen, M.K.; Makovicky, E.; Karup-Møller, S. Exploratory studies on substitutions in tennantite-tetrahedrite solid solution. Part IV. Substitution of germanium and tin. *Neues Jahrb. Miner. Abh. J. Miner. Geochem.* **2003**, *179*, 43–71. [CrossRef]
29. Klünder, M.H.; Karup-Møller, S.; Makovicky, E. Exploratory studies on substitutions in the tetrahedrite-tennantite solid solution series Part III. The solubility of bismuth in tetrahedrite-tennantite containing iron and zinc. *Neues Jahrb. Miner. Mon.* **2003**, *2003*, 153–175. [CrossRef]
30. George, L.L.; Cook, N.J.; Ciobanu, C.L. Partitioning of trace elements in co-crystallized sphalerite–galena–chalcopyrite hydrothermal ores. *Ore Geol. Rev.* **2016**, *77*, 97–116. [CrossRef]
31. Foit, F.F., Jr.; Hughes, M.J. Structural variations in mercurian tetrahedrite. *Am. Mineral.* **2004**, *89*, 159–163. [CrossRef]
32. Johnson, M.L.; Burnham, C.W. Crystal structure refinement of an arsenic-bearing argentian tetrahedrite. *Am. Mineral.* **1985**, *70*, 165–170.
33. Johnson, N.E.; Craig, J.R.; Rimstidt, J.D. Crystal chemistry of tetrahedrite. *Am. Mineral.* **1988**, *73*, 389–397.
34. Pattrick, R.A.D.; Hall, A.J. Silver substitution into synthetic zinc, cadmium and iron tetrahedrites. *Mineral. Mag.* **1983**, *47*, 441–451. [CrossRef]
35. Charnock, J.M.; Garner, C.D.; Pattrick, R.A.D.; Vaughan, D.J. Co-ordination sites of metals in tetrahedrite minerals determined by EXAFS. *J. Solid State Chem.* **1989**, *82*, 279–289. [CrossRef]
36. Charnock, J.M.; Garner, C.D.; Pattrick, R.A.D.; Vaughan, D.J. EXAFS and Mössbauer spectroscopic study of Fe-bearing tetrahedrites. *Mineral. Mag.* **1989**, *53*, 193–199. [CrossRef]
37. Pattrick, R.A.D.; van der Lann, G.; Vaughan, D.J.; Henderson, C.M.B. Oxidation state and electronic configuration determination of copper in tetrahedrite group minerals by L-edge X-ray absorption spectroscopy. *Phys. Chem. Miner.* **1993**, *20*, 395–401. [CrossRef]
38. Oen, I.S.; Kieft, C. Bismuth-rich tennantite and tetrahedrite in the Mangualde pegmatite, Viseu district, Portugal. *Neues Jahrb. Miner. Mon.* **1976**, *2*, 94–96.
39. Bortnikov, N.S.; Kudryavtsev, A.S.; Troneva, N.V. Bi-rich tetrahedrite from the Tary-Ekan deposit (East Karamazar, central Asia). *Mineral. Zhurnal* **1979**, *198*, 61–64. (In Russian)
40. Kieft, K.; Eriksson, G. Regional zoning and metamorphic evolution of the Vindfall Pb-Zn ore, east central Sweden. *GFF* **1984**, *106*, 305–317. [CrossRef]
41. Spiridonov, E.M.; Chvileva, T.N.; Borodaev, Y.S.; Vinogradova, R.A.; Kononov, O.V. The influence of bismuth on optical properties of gray copper. *Dokl. Akad. Nauk SSSR* **1986**, *290*, 1475–1478. (In Russian)
42. Breskovska, V.V.; Tarkian, M. Compositional variation in Bi-bearing fahlores. *Neues Jahrb. Miner. Mon.* **1994**, *5*, 230–240.
43. Gołębiowska, B.; Pieczka, A.; Parafiniuk, J. Substitution of Bi for Sb and As in minerals of the tetrahedrite series from Rędziny, Lower Silesia, southwestern Poland. *Can. Mineral.* **2012**, *50*, 267–279. [CrossRef]
44. Nash, J.T. Geochemical studies in the Park City District; II, Sulfide mineralogy and minor-element chemistry, Mayflower Mine. *Econ. Geol.* **1975**, *70*, 1038–1049. [CrossRef]
45. Basu, K.; Bortnykov, N.; Mookherjee, A.; Mozgova, N.; Tsepin, A.I. Rare minerals from Rajpura-Dariba, Rajasthan, India III: Plumbian tetrahedrite. *Neues Jahrb. Miner. Abh.* **1981**, *141*, 280–289.
46. Mozgova, N.N.; Tsepin, A.I. *Fahlore (Features of Chemical Composition and Properties)*; Nauka: Moscow, Russia, 1983; p. 279. (In Russian)
47. Moh, G.H. Sulfosalts: Observations and mineral descriptions, experiments and applications. *Neues Jahrb. Miner. Abh.* **1984**, *150*, 25–64.
48. Vavelidis, M.; Melfos, V. Two plumbian tetrahedrite-tennantite occurrences from Maronia area (Thrace) and Milos island (Aegean sea), Greece. *Eur. J. Mineral.* **1997**, *9*, 653–658.
49. Bishop, A.C.; Criddle, A.J.; Clark, A.M. Plumbian tennantite from Sark, Channel Islands. *Mineral. Mag.* **1977**, *41*, 59–63. [CrossRef]

50. Ixer, R.A.; Stanley, C.J. Silver mineralization at Sark's Hope mine, Sark, Channel Islands. *Mineral. Mag.* **1983**, *47*, 539–545. [CrossRef]
51. Förster, H.J.; Rhede, D.; Tischendorf, G. Continuous solid-solution between mercurian giraudite and hakite. *Can. Mineral.* **2002**, *40*, 1161–1170. [CrossRef]
52. Jurković, I.B.; Garašić, V.; Jurković, I.M. Geochemical characteristics of mercurian tetrahedrite, barite and fluorite from the Duboki Vagan, Glumac and Dubrave-Dugi Dol barite deposits, south of Kreševo, Mid-Bosnian Schist Mts. *Geol. Croat.* **2011**, *64*, 49–59. [CrossRef]
53. Basu, K.; Bortnykov, N.; Mookherjee, A.; Mozgova, N.; Sivtsov, A.V.; Tsepin, A.I.; Vrublevskaja, Z.V. Rare minerals from Rajpura-Dariba, Rajasthan, India V: The first recorded occurrence of a manganoan fahlore. *Neues Jahrb. Miner. Abh.* **1984**, *149*, 105–112.
54. Voropayev, A.V.; Spiridonov, E.M.; Shchibrik, V.I. Cd-Tetrahedrite, first find in the USSR. *Dokl. Acad. Sci. USSR* **1988**, *300*, 1446–1468.
55. Pattrick, R.A. Microprobe analyses of cadmium-rich tetrahedrites from Tyndrum, Perthshire, Scotland. *Mineral. Mag.* **1978**, *42*, 286–288. [CrossRef]
56. Pattrick, R.A. Pb-Zn and minor U mineralization at Tyndrum, Scotland. *Mineral. Mag.* **1985**, *49*, 671–681. [CrossRef]
57. Huiwen, J.D.F.Z.Z.; Chunpei, Z. The first Discovery of Cd-Freibergite in China. *Acta Mineral. Sin.* **1988**, *2*, 005.
58. Voudouris, P.C.; Spry, P.G.; Sakellaris, G.A.; Mavrogonatos, C. A cervelleite-like mineral and other Ag-Cu-Te-S minerals [Ag_2CuTeS and $(Ag, Cu)_2TeS$] in gold-bearing veins in metamorphic rocks of the Cycladic Blueschist Unit, Kallianou, Evia Island, Greece. *Mineral. Petrol.* **2011**, *101*, 169–183. [CrossRef]
59. Dobbe, R.T. Manganoan-cadmian tetrahedrite from the Tunaberg Cu-Co deposit, Bergslagen, central Sweden. *Mineral. Mag.* **1992**, *56*, 113–115. [CrossRef]
60. Kovalenker, V.A.; Rusinov, V.L. Goldfieldite: Chemical composition, parageneses and conditions of formation. *Mineral. Zhurnal* **1986**, *8*, 57–70. (In Russian)
61. Kase, K. Tellurian tennantite from the Besshitype deposits in the Sambagawa metamorphic belt, Japan. *Can. Mineral.* **1986**, *24*, 399–404.
62. Knittel, U. Composition and association of arsenian goldfieldite from the Marian gold deposit, Northern Luzon, Philippines. *Mineral. Petrol.* **1989**, *40*, 145–154. [CrossRef]
63. Shimizu, M.; Stanley, C.J. Coupled Substitutions in Goldfieldite-Tetrahedrite Minerals from the Iriki Mine, Japan. *Mineral. Mag.* **1991**, *55*, 515–551. [CrossRef]
64. Pohl, D.; Liessmann, W.; Okrugin, V.M. Rietveld analysis of selenium-bearing goldfieldites. *Neues Jahrb. Miner. Mon.* **1996**, *1996*, 1–8.
65. Pinto, A.; Ferreira, A.; Bowles, J.F.W.; Gaspar, O.C. Mineralogical and textural characterization of the Neves-Corvo ores. Metallogenetic implications. In *Geology and VMS Deposits of the Lberian Pyrite Belt*; Ser. 27; Baniga, F.J.A.S., Carvalho, D., Eds.; SEG Neves Corvo Field Conference: Lisbon, Portugal, 1997; p. 90.
66. Serranti, S.; Ferrini, V.; Masi, U.; Cabri, L.J. Trace-element distribution in cassiterite and sulfides from rubané and massive ores of the Corvo deposit, Portugal. *Can. Mineral.* **2002**, *40*, 815–835. [CrossRef]
67. Figueiredo, M.O.; Silva, T.P.; de Oliveira, D.P.S.; Rosa, D.R.N. Searching for In-carrier minerals in polymetallic sulphide deposits: Digging deeper into the crystal chemistry of indium chalcogenides. In *Digging Deeper, Proceedings of the 9th Biennial SGA Meeting, Ferrara, Italy, 29–31 August 2007*; Andrew, C.J., Ed.; Irish Association Economic Geologists: Dublin, Ireland, 2007; pp. 1355–1358.
68. McClenaghan, S.H.; Lentz, D.R.; Martin, J.; Diegor, W.G. Gold in the Brunswick No. 12 volcanogenic massive sulfide deposit, Bathurst Mining Camp, Canada: Evidence from bulk ore analysis and laser ablation ICP-MS data on sulfide phases. *Miner. Depos.* **2009**, *44*, 523–557. [CrossRef]
69. Gaspar, O.C. Mineralogy and sulfide mineral chemistry of the Neves-Corvo ores, Portugal: Insight into their genesis. *Can. Mineral.* **2002**, *40*, 611–636. [CrossRef]
70. Jurković, I.B.; Garašić, V.; Jurković, I.M. Cobalt, nickel, wolfram, cadmium, selenium, silver and gold-bearing mercurian tetrahedrite from the Saski Rad barite-siderite deposit in the Mid-Bosnian Schist Mts. *Geol. Croat.* **2011**, *64*, 223–237.
71. Wohlgemuth-Ueberwasser, C.C.; Viljoen, F.; Petersen, S.; Vorster, C. Distribution and solubility limits of trace elements in hydrothermal black smoker sulfides: An in-situ LA-ICP-MS study. *Geochim. Cosmochim. Acta* **2015**, *159*, 16–41. [CrossRef]

72. George, L.L.; Cook, N.J.; Crowe, B.B.P.; Ciobanu, C.L. Trace elements in hydrothermal chalcopyrite. *Mineral. Mag.* **2017**, in press.
73. Wilson, S.; Ridley, W.; Koenig, A. Development of sulphide calibration standards for the laser ablation inductively-coupled plasma mass spectrometry technique. *J. Anal. At. Spectrom.* **2002**, *17*, 406–409. [CrossRef]
74. United States Geological Survey. Microanalytical Reference Materials and Accessories. Available online: http://crustal.usgs.gov/geochemical_reference_standards/microanalytical_RM.html (accessed on 6 October 2016).
75. Van Achterbergh, E.; Ryan, C.; Jackson, S.; Griffin, W. Data reduction software for LA-ICP-MS: Laser-Ablation-ICPMS in the earth sciences—Principles and applications. *Mineral. Ass. Can.* **2001**, *29*, 239–243.
76. Danyushevsky, L.; Robinson, P.; Gilbert, S.; Norman, M.; Large, R.; McGoldrick, P.; Shelley, M. Routine quantitative multi-element analysis of sulphide minerals by laser ablation ICP-MS: Standard development and consideration of matrix effects. *Geochem. Explor. Environ. Anal.* **2011**, *11*, 51–60. [CrossRef]
77. Patten, C.; Barnes, S.J.; Mathez, E.A.; Jenner, F.E. Partition coefficients of chalcophile elements between sulfide and silicate melts and the early crystallization history of sulfide liquid: LA-ICP-MS analysis of MORB sulfide droplets. *Chem. Geol.* **2013**, *358*, 170–188. [CrossRef]
78. Cook, N.; Ciobanu, C.L.; George, L.; Zhu, Z.Y.; Wade, B.; Ehrig, K. Trace element analysis of minerals in magmatic-hydrothermal ores by laser ablation inductively-coupled plasma mass spectrometry: Approaches and opportunities. *Minerals* **2016**, *6*, 111. [CrossRef]
79. George, L.; Cook, N.J.; Cristiana, L.; Wade, B.P. Trace and minor elements in galena: A reconnaissance LA-ICP-MS study. *Am. Mineral.* **2015**, *100*, 548–569. [CrossRef]
80. Plotinskaya, O.Y.; Grabezhev, A.I.; Seltmann, R. Fahlores compositional zoning in a porphyry-epithermal system: Biksizak occurrence, South Urals, Russia as an example. *Geol. Ore Depos.* **2015**, *57*, 42–63. [CrossRef]
81. Buzatu, A.; Damian, G.; Dill, H.G.; Buzgar, N.; Apopei, A.I. Mineralogy and geochemistry of sulfosalts from Baia Sprie ore deposit (Romania)—New bismuth minerals occurrence. *Ore Geol. Rev.* **2015**, *65*, 132–147. [CrossRef]
82. Vokes, F.M. Geological studies on the Caledonian pyritic zinc-lead orebody at Bleikvassli, Norland, Norway. *Nor. Geol. Unders.* **1963**, *222*, 1–126.
83. Vokes, F.M. On the possible modes of origin of the Caledonian sulfide ore deposit at Bleikvassli, Nordland, Norway. *Econ. Geol.* **1966**, *61*, 1130–1139. [CrossRef]
84. Boulter, C.A.; Fotios, M.G.; Phillips, G.N. The Golden Mile, Kalgoorlie; a giant gold deposit localized in ductile shear zones by structurally induced infiltration of an auriferous metamorphic fluid. *Econ. Geol.* **1987**, *82*, 1661–1678. [CrossRef]